ABSTRACT

Title of Thesis: DOUBLE-EXPOSURE GRAY-SCALE PHOTOLITHOGRAPHY

Lance Adams Mosher, Master of Science, 2008

Directed by: Professor Reza Ghodssi
Department of Electrical and Computer Engineering

Three-dimensional (3D) photoresist structures may be realized by controlling the transmitted UV light intensity in a process termed gray-scale photolithography. Light modulation is accomplished by diffraction through sub-resolution pixels on a photomask. The number of photoresist levels is determined by the number of different pixel sizes on the mask, which is restricted by mask fabrication. This drawback prevents the use of gray-scale photolithography for applications that need a high vertical resolution.

The double-exposure gray-scale photolithography technique was developed to improve the vertical resolution without increasing the number of pixel sizes. This is achieved by using two gray-scale exposures prior to development. The resulting overlay produces an exposure dose that is a combination of both exposures. Calibration is utilized to relate the pixel sizes and exposure times to the photoresist height. This calibration enables automated mask design for arbitrary 3D structures and investigation of other effects, such as misalignment between the exposures.

DOUBLE-EXPOSURE GRAY-SCALE PHOTOLITHOGRAPHY

By

Lance Adams Mosher

Thesis submitted to the Faculty of the Graduate School of the
University of Maryland, College Park in partial fulfillment
of the requirements for the degree of
Master of Science
2008

Advisory Committee:
Professor Reza Ghodssi, Chair
Professor Martin Peckerar
Professor John Melngailis

Dedication

To my wife Dana for her unconditional love, patience, and support,
and to my parents, who provided the foundation for all I accomplish.

Acknowledgments

I would like to acknowledge Professor Reza Ghodssi for his support and guidance. He enabled me to conduct this research, and provided the advice and critiques necessary for me to complete this work.

I would also like to thank my predecessors, Dr. Brian Morgan and Dr. C. Mike Waits of the US Army Research Laboratory. By standing on the shoulders of these giants, I found success.

The work for this thesis was conducted at the US Army Research Laboratory, the Laboratory for Physical Sciences, and the FabLab at the University of Maryland. I would like to thank the cleanroom staff at these facilities, particularly Manrico Mirabelli, Steve Brown and Jonathan Hummel. I also thank Kevin Larson at Northrop Grumman for mask fabrication.

This research was supported by the Army Research Laboratory Collaborative Technology Alliance (CTA) Power and Energy program (Cooperative Agreement DAAD19-01-2-0010) and also by NASA Goddard Space Flight Center.

Finally, I would like to thank my friends and colleagues of the MEMS Sensors and Actuators Laboratory (MSAL) for their help and technical discussions throughout this process.

Table of Contents

List of Figures

Chapter 1

Introduction

1.1 Introduction to MEMS

Since the invention of the solid state transistor, the integrated circuit (IC) industry has reaped many benefits by miniaturizing and streamlining the fabrication process for electronic devices. However, the size of some technologies was still limited by their mechanical components. The continued trend for miniaturization resulted in the development of micro-electro-mechanical-systems (MEMS). These devices, or systems, are typically micrometer-scaled mechanical sensors and actuators integrated directly with electronic components on a single chip. Like ICs, miniaturization of sensors and actuators can significantly decrease production costs due to advantages in parallel processing. However, devices may also benefit from "scaling laws" as the ratio between the surface area and volume increases. In some cases, these scaling effects make MEMS devices more efficient and sensitive while consuming less power than the corresponding macro-scale counterparts. Some examples of commercially successful MEMS devices include accelerometers for collision detection, gyroscopes for inertial measurement units (IMU) and optical switches for digital light processing (DLP) technology. MEMS is an

interdisciplinary research area with applications in many scientific fields, including biotechnology, medicine, optics, communications, radio-frequency electronics, motors and power generation. However, there are still limitations in MEMS fabrication, such as realizing three-dimensional (3D) structures. The objective of this thesis is to exposure a robust fabrication technique to create 3D profiles with a high vertical resolution.

The following subsections describe materials and processes involved in MEMS fabrication. Photolithography and bulk and surface micromachining are presented, followed by a brief introduction to three-dimensional fabrication.

1.2 Fabricating MEMS

Silicon fabrication technology already developed for the IC industry served as the starting point for MEMS fabrication. The silicon wafers used in ICs provided good electrical and mechanical characteristics for MEMS and the tools used for machining these wafers were already available and well understood. Most MEMS devices still use silicon today for this very reason, but as the role of MEMS has evolved, the fabrication materials have also broadened to include those better suited for optics, biocompatibility and other applications.

One of the fundamental steps in MEMS fabrication is photolithography, which uses light to pattern a polymer layer on the wafer surface. After patterning, wafers are usually processed using either surface micromachining [1] or bulk micromachining [2]. Surface micromachining involves depositing and patterning material on the substrate, while bulk micromachining builds devices into the substrate itself. These processes will be described in the following subsections.

1.2.1 Photolithography

Photolithography is a three-step process of deposition, exposure and development. The process is used to pattern a layer of photosensitive polymer, called photoresist. This photoresist then acts as a masking layer for subsequent steps that either add or remove material to the device. The patterned photoresist is then either dissolved or, less commonly, used as a structural material.

Photoresist consists of a solvent and a photoactive compound (PAC). The solvent keeps the material in a viscous liquid form until deposition, where it evaporates causing the photoresist to solidify [3]. The solubility of the photoresist in a developing solution is controlled by the ultra-violet (UV) light-sensitive PAC. The reaction of the PAC to UV light depends on the tone of the photoresist. With positive tone photoresist, light forms scissions in the polymer chain, making it more soluble in an alkaline solution. The reaction is the opposite for negative tone photoresist, where UV light crosslinks the polymer, making it less soluble.

The photoresist is deposited as a thin (typically 1-10 µm) layer on the wafer using a spin or spray coating tool (Figure 1.1a). It is then exposed in a photolithography tool, where light is spatially patterned using an optical mask as shown in Figure 1.1b. The mask is usually chrome-on-quartz for micron or submicron features or printed on transparency for feature sizes ranging tens of microns. Finally, development in an alkaline solution for several minutes dissolves the soluble material (Figure 1.1c). This leaves a patterned "plane" of horizontal photoresist, parallel to the silicon "plane." Hence, photolithography is described as a planar or binary process.

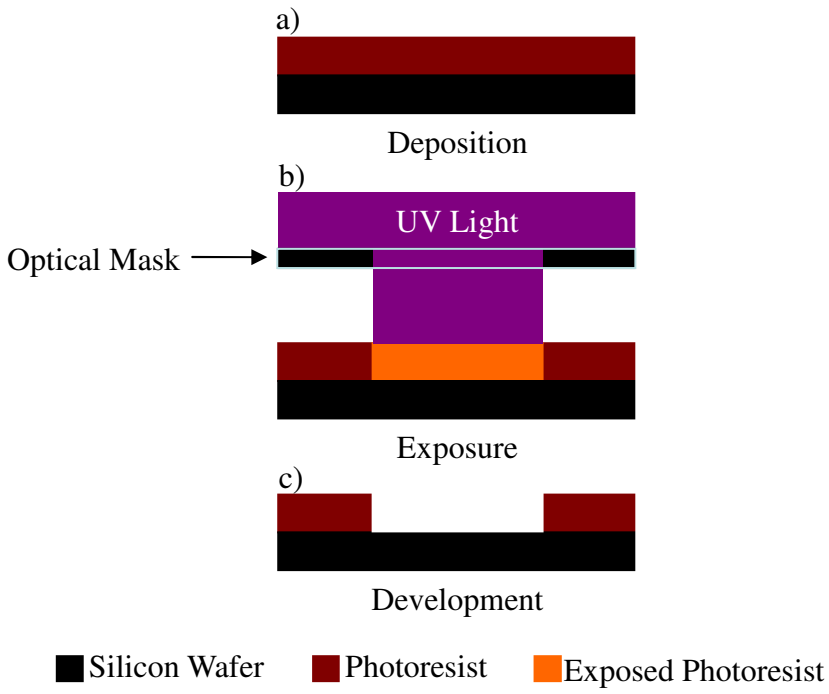

Figure 1.1: Three steps of the photolithography process with positive tone photoresist: (a) photoresist is deposited on the wafer by spray or spin coating, (b) the photoresist is exposed with UV light through an optical mask, and (c) the exposed photoresist is developed in an alkaline solution.

Exposure is the most important step and can be performed in a contact exposure system or a projection photolithography system (Figure 1.2a). With contact photolithography, the mask is in very close proximity or even direct contact with the wafer for feature sizes as small as 1 µm for many systems. Contact photolithography is common for larger MEMS devices that require whole-wafer patterns. However, contact exposure tools often require manual wafer loading and alignment, making the process serial. Since the mask directly contacts the photoresist, it must be cleaned after every use. As a result, contact photolithography is not widely used in commercial mass production.

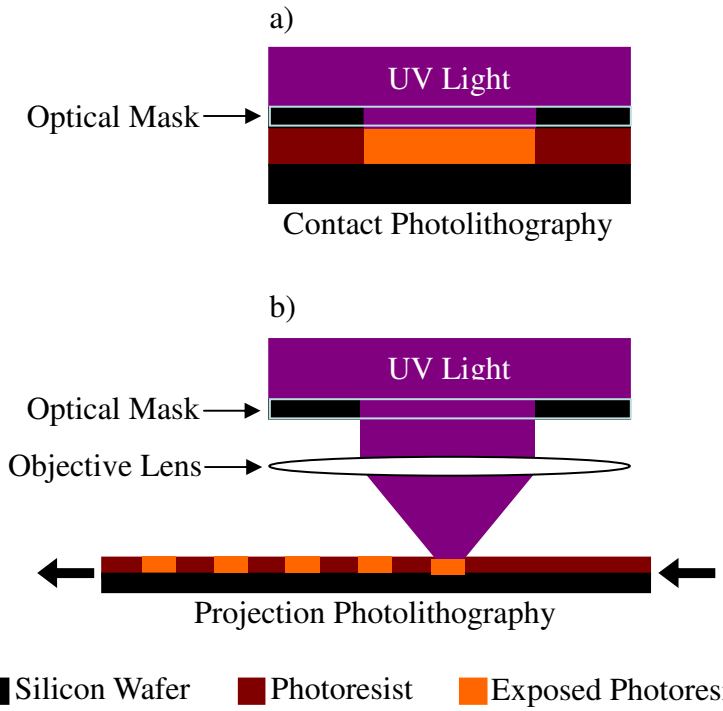

Figure 1.2: (a) Contact photolithography places the mask directly over the entire wafer for a 1:1 pattern transfer. (b) Projection photolithography uses an objective lens to reduce the image by 5x (in this example) and steps the mask pattern across the wafer.

Projection photolithography is typically performed in a wafer stepper, where the mask is optically reduced and projected onto the wafer using an objective lens as shown in Figure 1.2b. Instead of patterning the entire wafer in one exposure, the mask is exposed multiple times across the wafer surface, patterning one die at a time. Reduction helps achieve submicron feature sizes, but limits the die size of the wafer. However, typical MEMS devices are smaller than this die size, so this is not usually an issue. Projection systems typically reduce the mask by 5X or 4X, but some older systems use 10X and emerging systems use 1X. Projection photolithography is often a batch process because multiple wafers can be exposed in a single run of the tool. Batch processing is available in projection tools that utilize an automatic wafer handling system, which will automatically remove a wafer from a container, align the wafer on the stage, and return the wafer to another container after exposure. In addition, the mask is also handled automatically and never touches the wafer, thus it does not need to be cleaned after exposure. Because of the advantages in parallel processing, projection photolithography is widely used for commercial MEMS fabrication.

1.2.2 Surface Micromachining

Surface micromachining processes are generally used to fabricate thin-film MEMS devices by depositing and removing material on the surface of the substrate. Devices utilizing surface micromachining include microfluidic channels and suspended structures, such as cantilever beams. A typical surface process is shown

in Figure 1.3a, where a structural material is deposited in a thin layer over the entire wafer. To pattern this layer, a photoresist mask is deposited and patterned on top. An etch process is then used to remove the exposed material and finally the photoresist mask is removed, leaving the patterned film. Another key fabrication technique is sacrificial etching [4]. In this process, a sacrificial layer is first deposited and patterned using the deposition, photoresist patterning, etching and photoresist removal steps outlined above. Then, a structural layer is deposited on top and again patterned using the four steps. However, once both layers are patterned, the sacrificial layer is selectively etched away, which leaves the suspended structural layer intact as shown in Figure 1.3b.

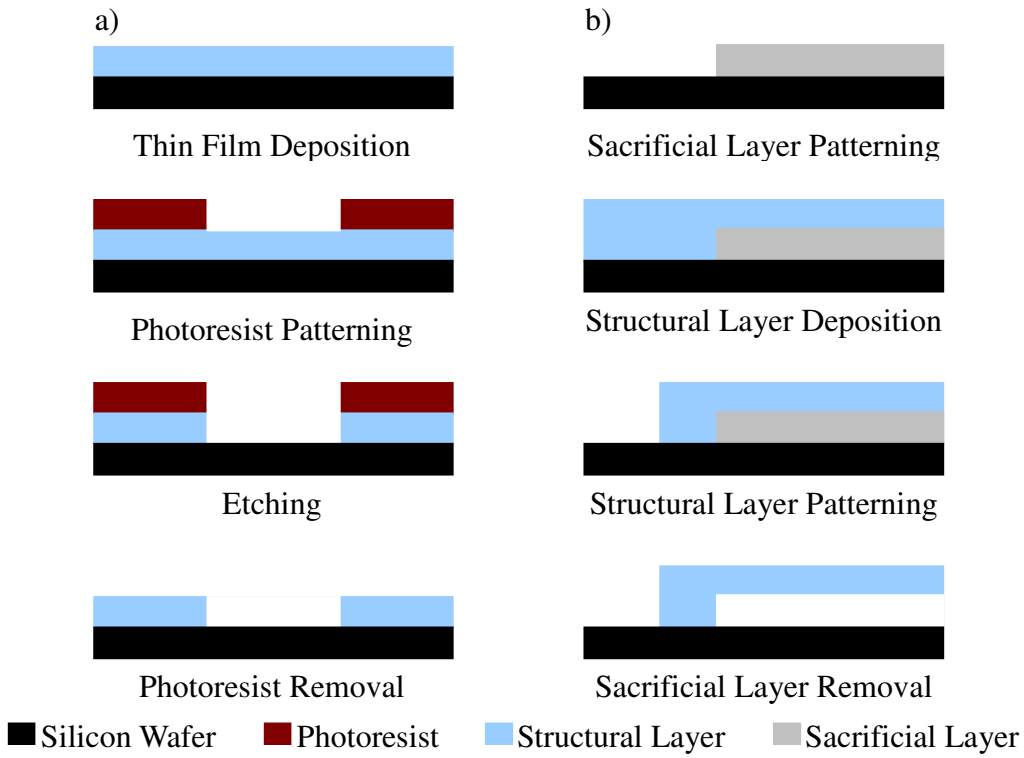

Figure 1.3: (a) Process to pattern a thin film layer. (b) The patterning steps are applied twice to fabricate a released structure using sacrificial etching.

1.2.3 Bulk Micromachining

Bulk micromachining [2] is used to fabricate structures within the bulk of the wafer by silicon etching. Removal of the bulk material forms structures such as membranes, trenches and holes. As with surface micromachining, photolithography is used to form a masking layer. After the photoresist is patterned on the wafer surface, the unprotected silicon is etched, leaving the desired pattern. There are a variety of wet and dry etching processes, which may be isotropic or anisotropic in nature. A wet process involves submerging the entire wafer in an etch chemical, and a dry process involves processing the wafer inside a plasma chamber.

1.2.3.1 Isotropic Etching

An isotropic etching process removes material in every direction at an equal rate. Typical masking materials, such as silicon dioxide, are unaffected by the etching and as a result the process removes silicon under the SiO_2. Isotropic etching is often used when undercutting is desired to release suspended structures. Wet and dry etching both produce similar profiles, as shown in Figure 1.4a. A typical wet process uses a combination of nitric acid, hydrofluoric acid and acetic acid, called HNA and a typical dry process uses a vapor-phase xenon difluoride. In both cases the etch process involves a chemical reaction with silicon, producing a volatile that is desorbed from the etched surface.

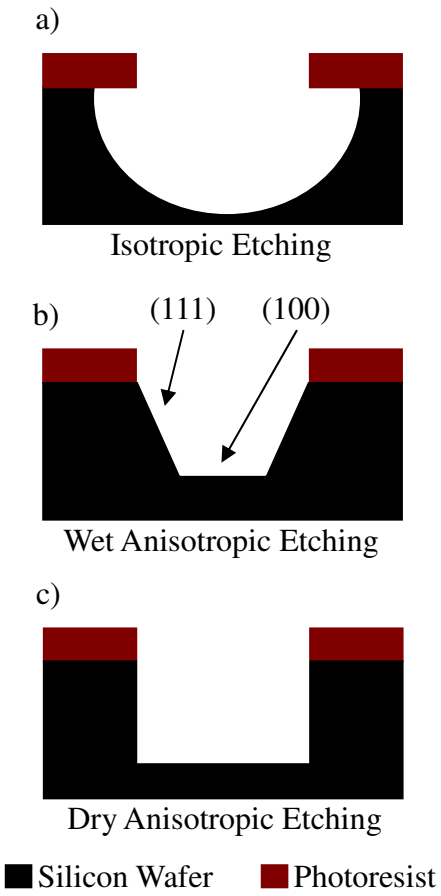

Figure 1.4: Cross-section view of a typical profile using (a) isotropic etching, (b) wet anisotropic etching and (c) dry anisotropic etching.

1.2.3.2 Anisotropic Etching

Anisotropic etching, in contrast to isotropic etching, removes material at a different rate depending on the direction. This results in a predictable sidewall angle, which is desirable for many MEMS devices. Anisotropic etching can be achieved using both wet and dry processes that produce different sidewall profiles. Wet anisotropic etching (Figure 1.4b) removes material from each crystal

orientation at a different rate. As an example, the etch rate of the (100) crystal plane is typically about 100 times the etch rate of the (111) crystal plane. The angles between each plane are constant, but etch profiles can be achieved by using wafers with different orientations. There are a variety of anisotropic etching solutions, including potassium hydroxide (KOH), tetramethylammonium hydroxide (TMAH), and ethylene diamine pyrocatecol (EDP). While wet anisotropic etching provides less profile control than isotropic etching, it is highly repeatable and can produce very smooth sidewalls with high etch rates. The fast etch rate makes it ideal for releasing large area structures and the repeatable sidewall angle makes it ideal for trench etching.

Dry anisotropic etching is performed using either reactive ion etching (RIE) or deep reactive ion etching (DRIE) [5, 6]. In both cases, the objective is to etch vertical sidewalls as shown in Figure 1.4c. This process can also be used for surface micromachining to etch thin layers of silicon dioxide or silicon nitride, but the etching gasses are different than for silicon etching. Wafer patterning is performed using photolithography. Silicon etches at a different rate than photoresist and the ratio between the etch rates is termed the etch selectivity. The wafer is placed in a vacuum chamber on a large plate electrode with a similar electrode above. Etch gasses are introduced and an electric field creates a plasma and energizes ions, accelerating them towards the wafer. Two etching mechanisms occur; first the highly directional ions sputter the silicon surface and etching species chemically

remove the silicon. The first mechanism is anisotropic, while the latter is generally isotropic. Horizontal surfaces are roughened by sputtering, which increases the rate of chemical etching and makes the etch process more isotropic. In order to achieve deeper etch depths, passivation on the sidewalls is required to prevent or inhibit lateral etching. For example, DRIE enables etches through the entire wafer using repeated cycles of etching and passivation, called the Bosch process [7]. After each etching cycle, a passivation layer is deposited covering the entire surface. Sputtering from the next etch cycle is vertical, so it quickly removes the passivation on the bottom. This opens up the horizontal surfaces to chemical etching, while protecting the sidewalls. Etch rates as high as 4 μm have been demonstrated using DRIE [8], with a selectivity as high as 130:1 [9].

1.3 Literature Review: Three-Dimensional Fabrication

The fabrication technology described above provides great control over in-plane dimensions. While other fabrication techniques exist, the above methods are available to most MEMS designers. These common techniques provide little to no ability to realize arbitrary features in the vertical direction, which significantly restricts out-of-plane fabrication. Sidewall profiles are essentially limited to either nearly vertical, fixed angles or undercut, which are formed by dry anisotropic etching, wet anisotropic etching and isotropic etching, respectively.

Three-dimensional fabrication is not a requirement for IC fabrication; however, it has become very important as MEMS expands on the initial set of tools adopted from the IC industry. MEMS designers who seek to miniaturize more mechanical and electrical devices on the micrometer scale are often limited by the planar nature of more traditional IC-based fabrication technology. In order for MEMS technology to meet the demand for this miniaturization, there must be a robust fabrication technology that is capable of fabricating structures with an arbitrary sidewall profile. However, one of the many benefits to miniaturization is that MEMS devices are cheaper to produce because parallel fabrication allows multiple devices to be created on a single wafer. Therefore any new 3D fabrication methods must also be compatible with existing MEMS technology and parallel processing to be commercially viable.

With the emergence of new 3D MEMS applications, several 3D fabrication technologies have been developed. One of the most promising 3D methods is 3D photolithography. As previously mentioned, common binary photolithography is a widely accepted and powerful patterning technology, but the binary exposures restrict photoresist to planar geometries. Three-dimensional photolithography techniques alleviate this restriction by enabling enhanced control over the photoresist profile. This method has been demonstrated in optics [10-12], where 3D lenses exhibit greater performance. For example, the phase Fresnel lens in [12] can

be realized as a phase zone plate using only planar technology, but it will have a diminished efficiency compared to a 3D phase Fresnel lens. Other applications of 3D photolithography include microfluidics [13] for microchannels, microsurgical tools [14], and photonic crystals [15].

In contrast to binary photolithography (Figure 1.5a), 3D photolithography methods use a variable-intensity exposure to produce vertically shaped photoresist profiles (Figure 1.5b). Commonly, 3D photolithography is achieved by gray-scale or gray-tone photolithography [16], which uses a variable-dose exposure to control the development depth in photoresist. In traditional planar photolithography, the dose selected is always greater the dose-to-clear, or clearing dose, which fully exposes the photoresist down to the silicon. The variable dose in gray-scale photolithography is always a partial exposure less than the dose-to-clear.

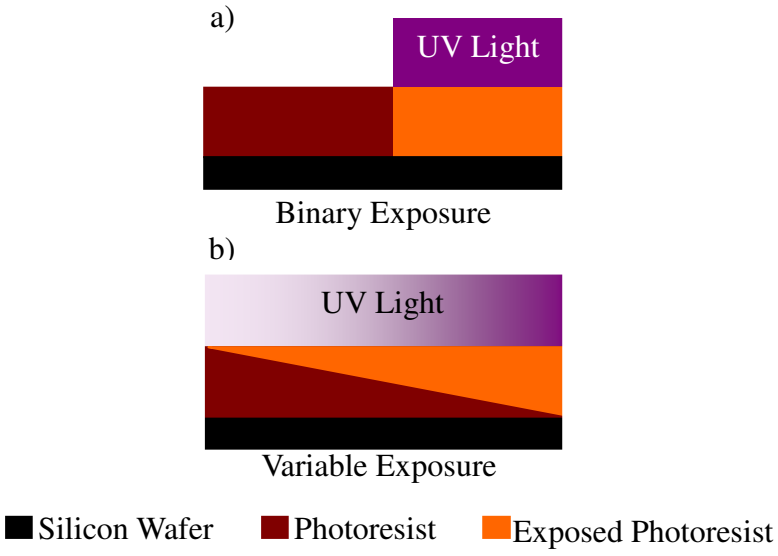

Figure 1.5: Cross-section view of exposure profile using (a) binary exposure and (b) variable exposure. The right side of both (a) and (b) receive the most intense UV light, represented by dark violet.

Each unique exposure dose will create a corresponding photoresist thickness, termed a gray level, after the development step. A higher dose results in a lower gray level for positive tone materials. As with binary photolithography, the remaining 3D pattern can then be either transferred into a substrate via a masking process [17] or used as the structural material itself. Sources in the literature tend to define gray-scale photolithography differently. This thesis defines gray-scale photolithography as any technique that uses a variable exposure to produce 3D photoresist profiles.

Current 3D photolithography technologies can be separated into three primary groups. The first involves multiple-step photolithography using binary transmission masks, the second group uses maskless direct-beam writing, and the third group uses variable-transmission gray-scale masks. Each photolithography technique has advantages and disadvantages that make them suited to different applications.

1.3.1 Multiple-Step Photolithography

Several groups have presented multiple-step photolithography fabrication with positive photoresist [18] and negative photoresist with applications in microfluidic channels [13] and photonic crystals [15]. The photoresist is treated with a binary exposure pattern using a dose at or below the clearing dose. Multiple planar, or binary-transmission, masks are exposed with different doses, resulting in

a unique photoresist height for each mask. For example, a wafer is first exposed with the clearing dose, and then two more subsequent exposures using partial doses of 60% and 30% of the clearing dose. A different mask is used for each exposure, creating the step profile shown in Figure 1.6. The exposure dose for each mask is usually controlled by adjusting either the exposure time or the exposure intensity to achieve the desired photoresist height. As demonstrated in the literature, each mask adds an additional gray level, so *n* masks produces *n* +1 levels. Theoretically, it is possible to increase the number of levels per mask by overlapping exposures, but this has not yet been demonstrated in the literature.

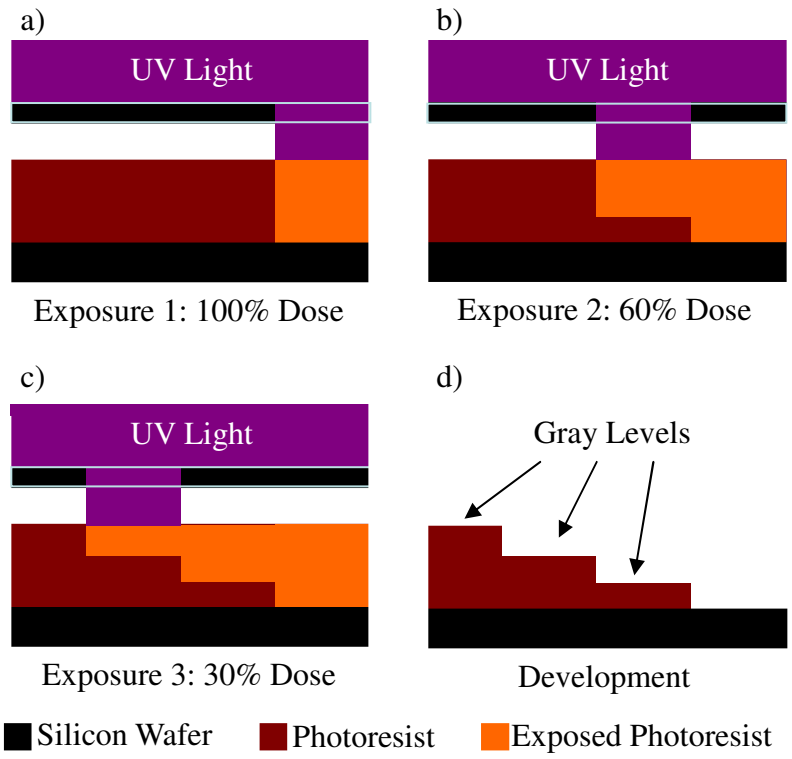

Figure 1.6: Cross-sectional views of a multiple-step photolithography process with three steps. (a) The first step uses the full dose, just like a traditional photolithography process. (b) The second and third exposures used a smaller dose, controlled by either decreasing the write time or the UV exposure intensity. (d) The final stepped pattern is revealed after development.

Chung et al. described a novel additional step, which introduced a gray-scale exposure from the back side of the photoresist [18]. Thin titanium layers were deposited on a transparent wafer, followed by photoresist. By exposing from the back side of the wafer, the titanium masks the light to pattern the photoresist from the back. Each titanium layer was a different thickness, which produced a different UV transmission that controlled the back-side dose. Each titanium thickness required an additional photolithography step, further complicating the procedure. However, by combining this back-side variable-dose exposure with the multiple partial exposures, this group fabricated suspended structures with 3D profiles on both sides.

Unfortunately, alignment limitations can be prohibitive for high dimensionality control, which requires many gray levels to achieve more continuous slopes. While multiple-step photolithography is compatible with existing photolithography tools, it is only effective for applications that require a simple vertical profile with a few steps.

1.3.2 Direct-Write Photolithography

Structures fabricated using direct-write photolithography, in contrast to multiple-exposure photolithography, have very smooth relief profiles and often have a better horizontal and vertical resolution. Maskless photolithography tools create 3D structures by directly exposing the photoresist with a finely focused beam

(Figure 1.7). Three-dimensional x-ray photolithography [19] has been demonstrated using an x-ray source and a binary mask pattern. The sample is rotated on a computer-controlled tilt stage, which controls the sidewall angle. Electron-beam [20-22] and ultraviolet [23] photo lithography utilize maskless exposure systems to deliver a programmed dose pattern to the photoresist. As each spot exposes the photoresist, the beam write time or exposure intensity is adjusted to control the dose and achieve variable-relief structures. Finally, 2-photon microsterolithography [19, 24-26] uses a tightly focused laser beam to expose structures within a photopolymerizable resin. Unlike other direct-write technologies, where the photoresist is exposed to a column of the writing beam, photopolymerization (solidification) only occurs in very close proximity to the focal spot of the writing beam. This allows geometries of great complexity to be fabricated.

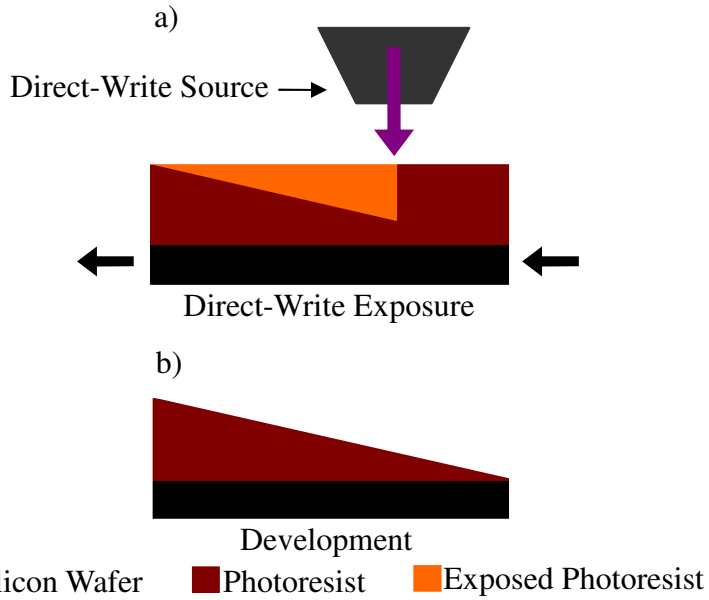

Figure 1.7: Cross-section of direct-write photolithography. (a) The exposure dose varies as the beam scans along the wafer. (b) After the exposure is completed, development reveals the smoothly sloping profile.

While the above lithographic techniques enable realization of a wider variety of structures compared to multiple-exposure photolithography, longer fabrication times and the need for specialized equipment makes this technology less applicable when high throughput is required.

1.3.3 Gray-Scale Masks

Three-dimensional photolithography using a gray-scale mask [27-36] is capable of realizing structures with a higher vertical resolution than multiple-exposure photolithography while still using conventional photolithography tools. This process was first demonstrated and patented by Gal in 1994 [37]. Gray-scale mask photolithography is a similar technique to both traditional and multi-step photolithography in that it uses a photomask in a conventional exposure system to pattern photoresist (Figure 1.8). However, gray-scale masks contain variable-transmission patterns that transmit only part of the UV intensity. Therefore, the UV transmission pattern controls the dose delivered to the photoresist. The mechanism to control the UV intensity gradient in gray-scale photolithography varies with each technique and has been demonstrated with pixelated [27-33] and continuous-tone [34, 35] optical masks. Pixelated gray-scale masks use diffraction through many sub-resolution pixels to control the UV dose. Continuous-tone masks use a proprietary energy-beam sensitive mask material to directly write the optical density onto the mask, thereby controlling the UV absorption.

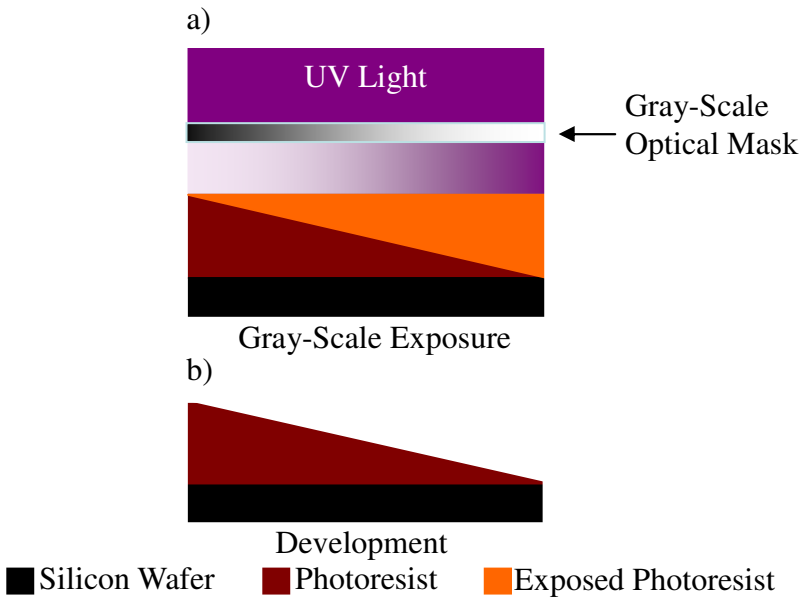

Figure 1.8: The gray-scale optical mask controls the UV light intensity across the wafer using a single exposure, resulting in a sloped profile. (a) The gradient pattern on the mask blocks most of the UV light on the left, and transmits the most UV light on the right. (b) The exposed resist is developed, leaving a sloped profile.

Both continuous-tone and pixelated masks can be used to fabricate structures on the order of tens of microns. Continuous-tone masks use a proprietary technology that is limited to five inch or six inch mask plates, which limits the wafer size using contact photolithography and the die size in projection photolithography. Conversely, pixelated gray-scale mask designs may be written with conventional mask writers and are compatible with any plate dimension. Pixelated masks are less restricted and, in many cases, more cost-effective to produce. Therefore, this research focuses on developing improved 3D fabrication capabilities using pixelated gray-scale masks.

1.3.4 Limitations of Pixelated Gray-Scale Photolithography

Pixelated masks are not suitable for all three-dimensional applications. While the technology is more desirable in some ways than continuous-tone masks, the vertical resolution is finite and only capable of producing tens of gray levels, compared to hundreds with continuous-tone gray-scale photolithography. This places pixelated gray-scale photolithography between multiple-step and continuous-tone techniques when comparing the vertical resolution. The cause of this limitation will be described in Chapter 2. Since only a finite number of gray levels are possible, 3D profiles that require smooth sidewalls can only be approximated using this technique. While this is sufficient for many devices, some applications for optics and power MEMS devices cannot be fabricated using pixelated technology. For example, the 3D microcompressor [17] cannot be fabricated because individual gray level steps along the slope will interrupt fluid flow and ruin device performance.

1.4 Thesis Objectives

As a solution, the objective of this research is to improve upon pixelated gray-scale photolithography to realize higher-resolution structures. This thesis describes the development and execution of a new photolithography technique, termed double-exposure gray-scale photolithography. This technique combines

multiple-step photolithography with pixelated gray-scale masks. Just as multiple exposure steps can extend the resolution of binary masks, the double-exposure technique can extend the resolution of pixelated gray-scale masks by the addition of a second exposure. The foundation of this work, pixelated gray-scale photolithography, will be described in detail in Chapter 2. Chapter 3 will present double-exposure gray-scale photolithography, including the theory, calibration, mask design, and fabrication steps. Results and discussion will follow in Chapter 4, outlining the fabrication results for structures realized using this technique. The discussion will contain an analysis of the mask alignment between the two exposures and present a possible solution. Concluding remarks will be provided in Chapter 5, including a discussion of future possibilities for double-exposure gray-scale technology.

Chapter 2

Pixelated Gray-Scale Photolithography

2.1 Introduction

The objective of this work is to investigate and evaluate a significant improvement to the pixelated gray-scale photolithography process. This chapter provides the background on pixelated gray-scale technology, including the two primary fabrication steps: creating the 3D photoresist layer with gray-scale photolithography and transferring this pattern into the underlying substrate by dry anisotropic etching. First, the theory and design of pixelated gray-scale masks are presented, followed by the fabrication process to realize 3D photoresist structures and the etching process for pattern transfer into silicon.

Pixelated gray-scale photolithography is compatible with common MEMS fabrication methods because it requires only standard photolithography tools. Unlike other methods presented, it requires no proprietary technology to fabricate masks and only uses a single photolithography step to realize gray levels in photoresist. As presented in Chapter 1, traditional photolithography creates planar

profiles using a binary transmission UV light while pixelated gray-scale photolithography creates sloping profiles using a variable-transmission mask.

2.1.1 Variable-Transmission

Pixelated masks achieve variable transmission by diffracting UV light in a projection photolithography tool. The mask contains millions of chrome pixels that are below the resolution of the projection tool as shown in Figure 2.1. As UV light passes through the pixels, it is diffracted and then passed through the projection optics. A diffraction pattern of many orders is generated, but only the zeroth order is transmitted by the objective lens. This filtering effect removes all spatial information from individual pixels and the transmitted signal contains only a modulated UV intensity, which is dependant on the size of the pixels on the mask. Since the pixel size controls the UV intensity, it also controls the photoresist height after development. This concept is illustrated in Figure 2.2 [28].

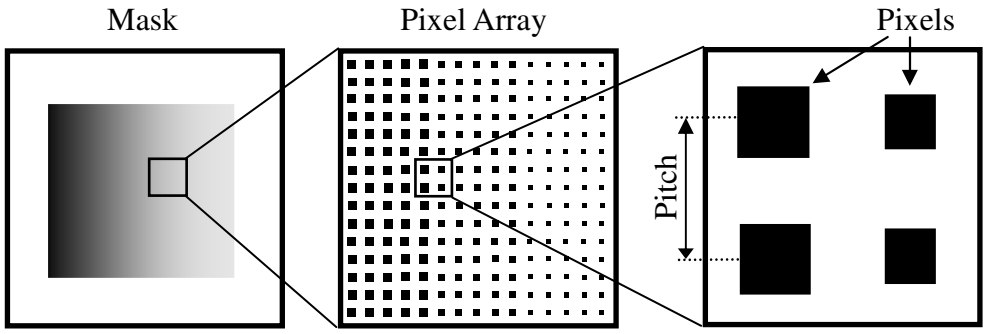

Figure 2.1: Top-down schematic of a pixelated gray-scale mask. Closer examination reveals the structure of the individual pixels.

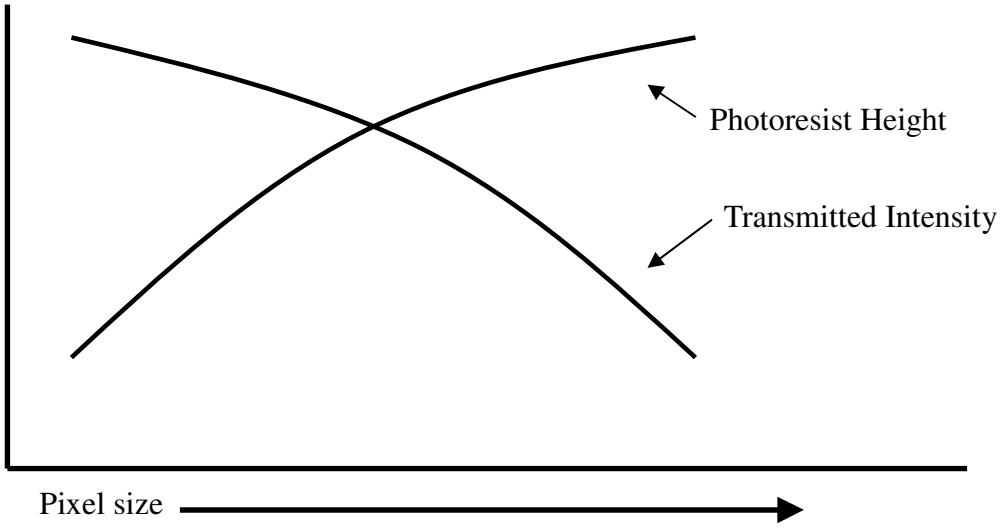

Figure 2.2: Conceptual graph illustrating the relationship between photoresist height and transmitted intensity with the pixel size. As the pixel size increases, the transmitted intensity decreases because more light is blocked. A decreasing intensity results in less exposure, and therefore higher photoresist.

2.1.2 Exposure Kinetics

When designing a pixelated mask, is important to first understand the relationship between the pixel size and the resulting photoresist height. The first step is to describe how the photoresist is exposed. This process differs for positive and negative-tone photoresist, but only positive photoresist was used in this work. The exposure kinetics of positive photoresist is governed by Beer's Law:

$$I(z) = I_s \exp(-\alpha \cdot z) . \tag{2.1}$$

Where $I(z)$ is the intensity at depth z, I_s is the intensity at the photoresist surface, and α is the absorption coefficient of the photoresist given in [38]. The photoresist is fully exposed when the dose, d, is greater than the dose-to-clear, E_0. The dose is defined with the exposure time, t, as:

$$d = I(z) \cdot t \tag{2.2}$$

The dose-to-clear is a well known property that specifies the minimum energy required to remove photoresist during development. By combining Equation 2.1 and 2.2 and solving for z:

$$z = \frac{1}{\alpha} \ln\left(\frac{t \cdot I_s}{d}\right). \tag{2.3}$$

Finally, the maximum development depth, z_{max}, can be obtained by substituting d for the dose-to-clear:

$$z_{\max} = \frac{1}{\alpha} \ln\left(\frac{t \cdot I_s}{E_0}\right). \tag{2.4}$$

Unfortunately, this theoretical approach is not sufficient to calculate the exposed depth using the tools available for this thesis because slight variations in

the photoresist deposition, development temperature, and humidity can also affect the final photoresist profile. In addition, the pixels on the mask push the resolution limits of the mask writer, creating unknown variation in the pixel size. This variation produces an unknown effect on the transmitted UV intensity. The projection photolithography tool also complicates a theoretical approach because it automatically scales the exposure time. This adjustment scales the actual exposure time to compensate for degradation of the lamp. For example, if the exposure time is entered as 2.0 seconds, the actual exposure time is adjusted and unknown. If the same exposure time is entered three weeks later, the actual exposure time will be different than before, and still unknown. However, the exposure time will be adjusted so that the dose of both exposures is the same. Since the exposure time is adjusted to maintain a constant dose, the "exposure time" is effectively an unknown unit of dose. This feature is convenient for maintaining process repeatability without needing to adjust the exposure time manually, but makes it very difficult to know the actual dose used for the exposure. As a solution, the entire process is calibrated using normalized values as demonstrated previously [28, 39-41].

2.1.3 Mask Calibration and Design

In this empirical calibration scheme, the dose is calculated and directly compared to the resulting photoresist height. The incident lamp intensity, I_0, is constant during the exposure, but the transmitted surface intensity, I_s, is dictated by the pixelated pattern on the mask. To compensate for unknowns in the exposure

time, a normalized surface intensity, I_n, was adopted that depends on the pixel fill factor, which is determined by the square pixel length, l, and the pitch, p, between pixels on the mask (Figure 2.1) [12]:

$$I_n = \frac{I_s}{I_0} = \frac{p^2 - l^2}{p^2}. \tag{2.5}$$

Calibration is performed by exposing a test pattern with known pixel sizes. Each pixel size will produce a corresponding gray level height in photoresist. The exposure time and development process are constant, so the only factor affecting the photoresist height is the normalized surface intensity, which depends only on the pixel size. The normalized intensity is compared to the corresponding gray level height and the empirical relationship is extracted using a numerical least-squares method [41]. This empirical relationship can then be applied to design mask layouts. Since the number of gray levels is limited, a desired structure can only be approximated by the available pixels as shown in Figure 2.3.

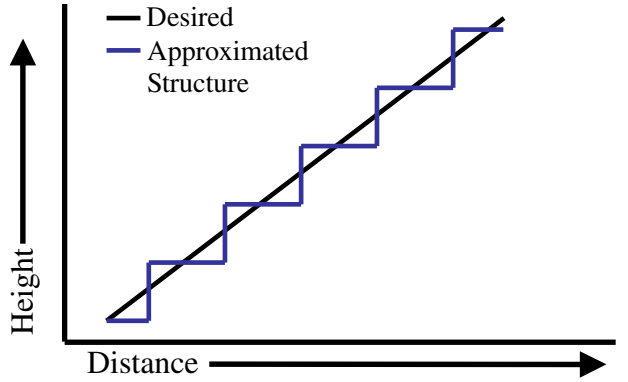

Figure 2.3: Conceptual profile view showing a desired structure and the approximated profile that would be created using pixelated photolithography.

2.2 Photolithography Process

Photolithography in this thesis is performed using projection photolithography, as described in Section 1.2.1. However, the process is much more sensitive than planar photolithography. Since pixelated gray-scale photolithography is a calibrated process, the type of photoresist, exposure, and development characteristics must remain constant for the calibration to be valid. The following subsections describe the selection process for the optimal photoresist type, exposure time, and development time.

2.2.1 Choosing a Photoresist

The type of photoresist was selected by the thickness on the wafer and the contrast [40]. Photoresist contrast describes the development rate of the photoresist as a function of the dose. When a photoresist is exposed, the development rate changes from the unexposed development rate (usually negligible) to the much higher exposed development rate. This change occurs when the dose transitions over the dose-to-clear. The slope of this transition between the unexposed development rate and the exposed development rate defines the contrast. High contrast photoresists have a narrow transition range are therefore more sensitive to changes in dose, while low contrast photoresists have a wider transition range. However, gray-scale photolithography is only compatible with dose values that are

within this transition range. Therefore, gray-scale photolithography is most flexible when used in conjunction with a low-contrast photoresist because the wider transition range allows more gray levels to be realized. This is the opposite for the IC industry, where an ideal photoresist has a high contrast for more vertical side walls. The photoresist selected for this research was Clariant's AZ9245. The contrast provides the ability to reproduce many gray levels, and is considered a thick photoresist, with nominal layer thicknesses ranging between 6 µm and 10 µm. When combined with a typical DRIE etch selectivity between 40 and 100, this enables realization of 3D structures ranging from tens to hundreds of micrometers tall [17].

2.2.2 Exposure Time

The exposure time determines the highest dose delivered to the photoresist. If the dose is too high, pixels that block almost incident intensity may still transmit enough light to completely expose the photoresist (Figure 2.4a). If the exposure time is too short, the smaller pixel sizes may not transmit enough and fail to expose the photoresist enough as shown in Figure 2.4b. The optimum exposure time is one that produces a gray level for each available pixel size on the mask. To optimize the exposure time, an exposure array is performed with the wafer stepper, which varies the exposure time for each die on the wafer. The wafer is then developed completely and the die with the most gray levels is selected as the ideal exposure time (Figure 2.4c).

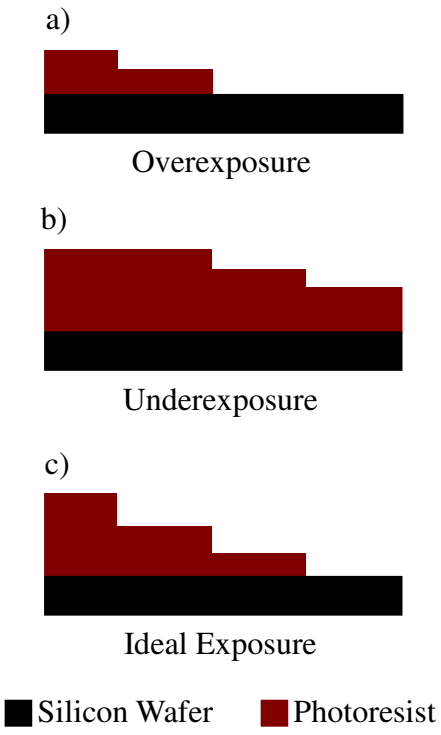

Figure 2.4: Profile view showing the same structure using different exposure times. Both (a) overexposure and (b) underexposure produce fewer gray levels than (c) the ideal exposure time.

There may be a range of exposure times that will produce a gray level for each pixel size on the mask. In this range, the exposure time determines the vertical distribution of gray levels within the photoresist. A higher exposure time will place all gray levels lower in the photoresist, while a lower exposure time achieves the opposite. The ideal exposure time depends on the desired structure in this case. This factor does provide some flexibility in the device design. For example, if a 3 µm linear wedge is designed, but later a 3.5 µm wedge is desired instead, it may be possible to simply decrease the exposure time to increase the thickness of the

structure. However, due to nonlinearity in the exposure, the wedge will not remain perfectly linear, as designed. Therefore, it is still desirable to keep all processing variables consistent for a particular mask design when possible.

2.2.3 Development Time

In contrast to planar photolithography, the development time is an important parameter in the pixelated gray-scale process. When developing planar structures, the only requirement is to remove all exposed photoresist. Unexposed photoresist is still removed by the developer, but at a drastically slower rate compared to exposed photoresist. Since photoresist thicknesses are on the order of micrometers, there is a generous tolerance for overdevelopment with planar photolithography. However, this is not the case for gray-scale photolithography. Gray levels are often designed with submicron thicknesses, so even a small degree of overdevelopment can wash away several gray levels. On the other hand, if the development time is too short, some exposed photoresist will remain and the structure will not be fully realized. The ideal development time is just long enough to reveal all gray levels, but short enough not to cause any overdevelopment.

Visually underdevelopment, ideal development and overdevelopment look identical to the underexposure, ideal exposure and overexposure depicted in Figure 2.4. This is because the two parameters are not independent. To some degree, overexposure can be balanced by underdevelopment and underexposure can be

balanced by overdevelopment to realize all gray levels. However, if overdevelopment is required to achieve the desired profile, development times can grow to more than an hour, compared to just five minutes in a normal photolithography process. Very long development times can result in a non-uniform development across the wafer as the developer concentration weakens over time. Therefore, it is desirable to choose a development time first and vary the exposure time until the desired photoresist profile is achieved at that development time.

2.3 Etching Process

The transfer of the 3D masking layer into silicon by etching is very similar to a standard DRIE method with a planar photoresist layer. The goal of the etch process is to transfer and amplify the 3D photoresist structure into silicon. However, as with the exposure and development steps, there are additional complications that require very tight control. This section describes the effect of the etch selectivity when etching 3D photoresist and the techniques applied to control etch selectivity.

2.3.1 Selectivity

As described in Section 1.2.3.2, the etch selectivity is the ratio between the silicon etch rate and the photoresist etch rate. In a typical planar DRIE process, the photoresist thickness is generally not a critical factor. In most cases, a high etch

selectivity is desired in order to use less photoresist. The photoresist thickness is selected to be thick enough to last until the desired etch depth is reached. Once this depth is achieved, the remaining photoresist is removed. However, for the gray-scale process the etch selectivity plays a much more important role as shown in Figure 2.5.

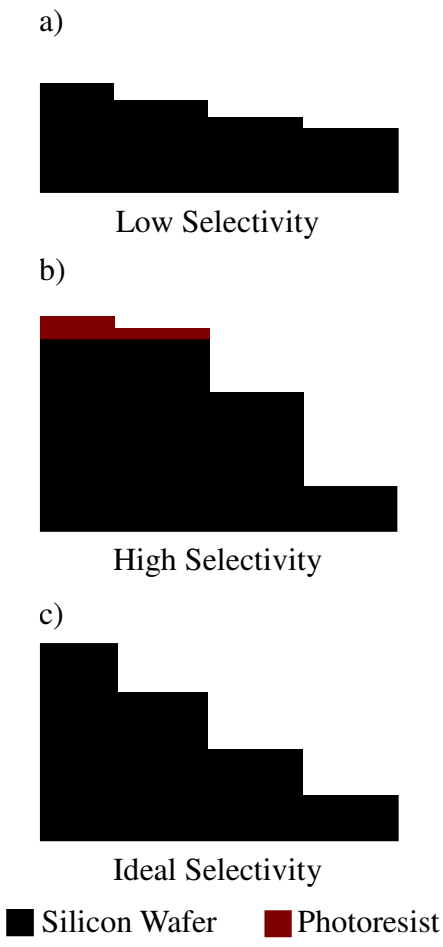

Figure 2.5: Profiles illustrating the effect of etch selectivity. (a) Low selectivity produces shorter step heights, while (b) not all gray levels are transferred if the selectivity is too high. (c) The ideal etch selectivity transfers the entire photoresist structure just as the photoresist is consumed.

If the selectivity is too low, the photoresist will be completely removed before the desired depth is achieved and the structure will not reach the desired height (Figure 2.5a). If the selectivity is too high, the desired depth will be realized before all of the photoresist has transferred (Figure 2.5b). Both the etch selectivity and the photoresist thickness must be controlled so that the desired etch depth is achieved just as the last photoresist is consumed, as shown in Figure 2.5c. Since a small increase in selectivity produces a large change in the final structure, it is often best to choose the selectivity first and then adjust the photolithography process to match this value.

2.3.2 Etch Selectivity Control

The selectivity can be controlled by varying several parameters in the DRIE tool. The most significant change occurs when either changing the directionality of the plasma or changing the concentration of ions. The electrode power in the chamber controls the directionality, where a higher power decreases the selectivity. This may seem counterintuitive, but by increasing the directionality of the ions the physical etch rate increases, which is the only rate that affects the photoresist. The chemical etch rate, which affects the silicon, does not change. The concentration of ions is partially controlled by the chamber pressure. When this increases, the selectivity also increases because there are more chemical etch species in the plasma to affect the silicon.

When shorter (< 40µm) 3D structures are desired, it may be necessary to reduce the etch selectivity below normal in order to allow all the gray levels to transfer. The control mechanisms described above are not sufficient to decrease the selectivity enough. The introduction of an oxygen step during the normal etch process helps alleviate this issue. A normal DRIE process switches between steps of etching and passivation. By adding a step of oxygen plasma acts to increase the photoresist etch rate because the oxygen acts as a physical etch, but lacks the chemical etch component that increases the silicon etch rate. The addition of this step has decreased the etch selectivity from 120 to 30 on the DRIE tool used with this research as shown in Figure 2.6 [12].

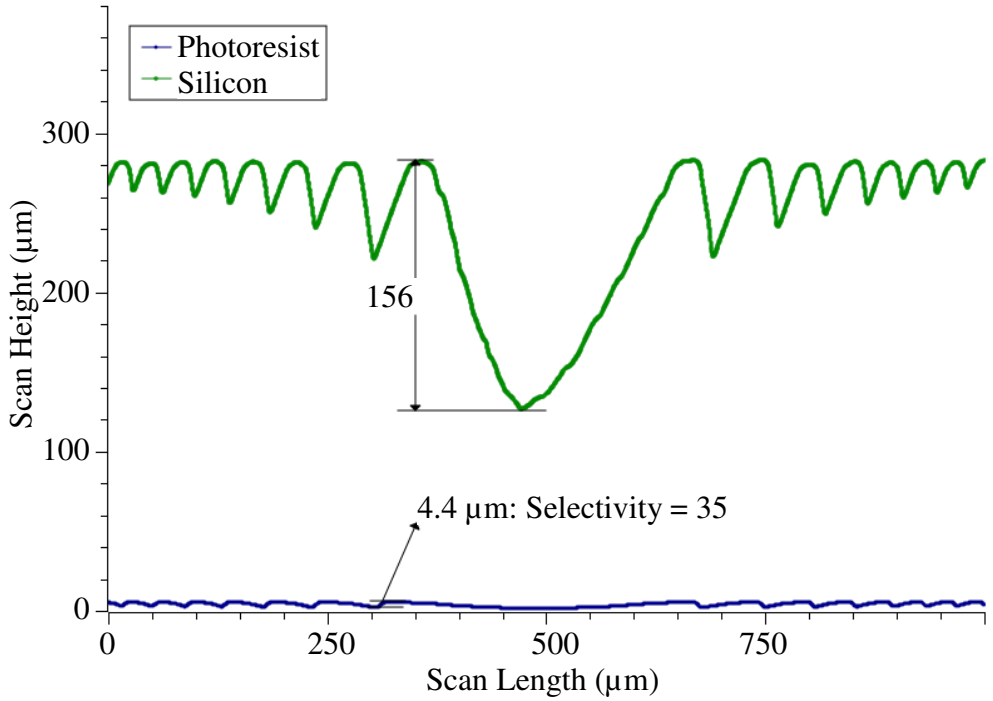

Figure 2.6: Example profilometer data from a Fresnel lens structure fabricated using gray-scale photolithography and a low selectivity DRIE process. An added oxygen plasma step has reduced the etch selectivity to 35.

2.4 Limited Vertical Resolution

As mentioned in Section 1.3.4, pixelated gray-scale masks are restricted to a finite number of gray levels. This is due to the limitations of the projection photolithography tool and the mask fabrication vendor. The projection system limits the maximum pixel size while the mask fabrication determines the minimum pixel size and pixel separation. Pixel sizes must be lower than the resolution of the projection tool. If pixel dimensions are greater than this limit, the diffractive effects will diminish and the individual pixels will begin to transfer into the photoresist, instead of a smooth gray level. The mask writing tool has a limited spot size and address size. The minimum spot size determines the smallest pixel size possible, while the address size limits the smallest increase in pixel size.

2.4.1 Pixel Size Limitation

The 5x reduction GCA stepper projection photolithography tool used for this research has a resolution of about 0.6 µm at the wafer level, which corresponds to a 3 µm maximum pixel size at the mask level. To achieve the smoothest gray levels possible, a pixel spacing of 2.6 µm and a maximum pixel size of 2.0 µm were selected. Pixels larger than this can produce some roughness in the sThe MEBES mask writing tool used to fabricate masks for this research has a minimum spot size of 0.6 µm and an address size of 0.1 µm. This means the smallest pixel size is 0.6

μm, with 0.1 μm steps between pixel sizes. After 0.6 μm, the next largest pixel size possible is 0.7 μm then 0.8 μm and so on. For simplicity, only square pixels were used in this research. Therefore, with these parameters, only fifteen pixel sizes are possible (0.6 μm to 2.0 μm with 0.1 μm between pixel sizes). Rectangular pixel geometries allow more gray levels, however less symmetric pixels may produce undesirable patterns, instead of smooth gray levels.

2.5 Summary

Pixelated gray-scale photolithography is a powerful and flexible 3D fabrication technology, where each pixel size on the mask produces a unique gray level in photoresist after development. An optimum exposure time and development time are selected for the desired process, and then an empirical calibration allows reliable prediction of the gray level each pixel size will produce. Then a mask can be fabricated to realize the desired 3D structures.

However, vendor and projection limitations restrict designs to only fifteen square pixel sizes. It is possible to increase the number of gray levels by using rectangular pixels, but only achieves tens of gray levels and may sacrifice surface smoothness. Therefore, it is desirable to increase the resolution of pixelated gray-scale lithography without changing the mask design process.

Chapter 3

Double-Exposure Gray-Scale Photolithography

3.1 Introduction

Double-exposure gray-scale photolithography was developed to realize 3D structures with greater morphology control. It was required to improve the vertical resolution of the fabrication technology compared to a single pixelated gray-scale exposure without altering the exposure or mask fabrication tools. Similar to multiple-step techniques, the process consists of multiple aligned exposures before development, but each exposure uses a gray-scale mask in place of a binary mask. Multiple-step photolithography has only been demonstrated using adjacent exposures. This means that even if several exposures are performed, each exposure is only targeted over unexposed photoresist. In contrast, double-exposure photolithography uses overlaid exposures, so that separate gray-scale exposures contribute to the final dose pattern. Two pixelated gray-scale exposures were used for this research and therefore the final dose is composed of the combination of both partial exposures. As described in Section 2.1.1, if *n* pixel sizes are used for a single pixelated exposure, it will produce *n* gray levels (Figure 3.1a). Double-

exposure photolithography will produce n^2 gray levels using the same number of pixel sizes as shown in Figure 3.1b [42].

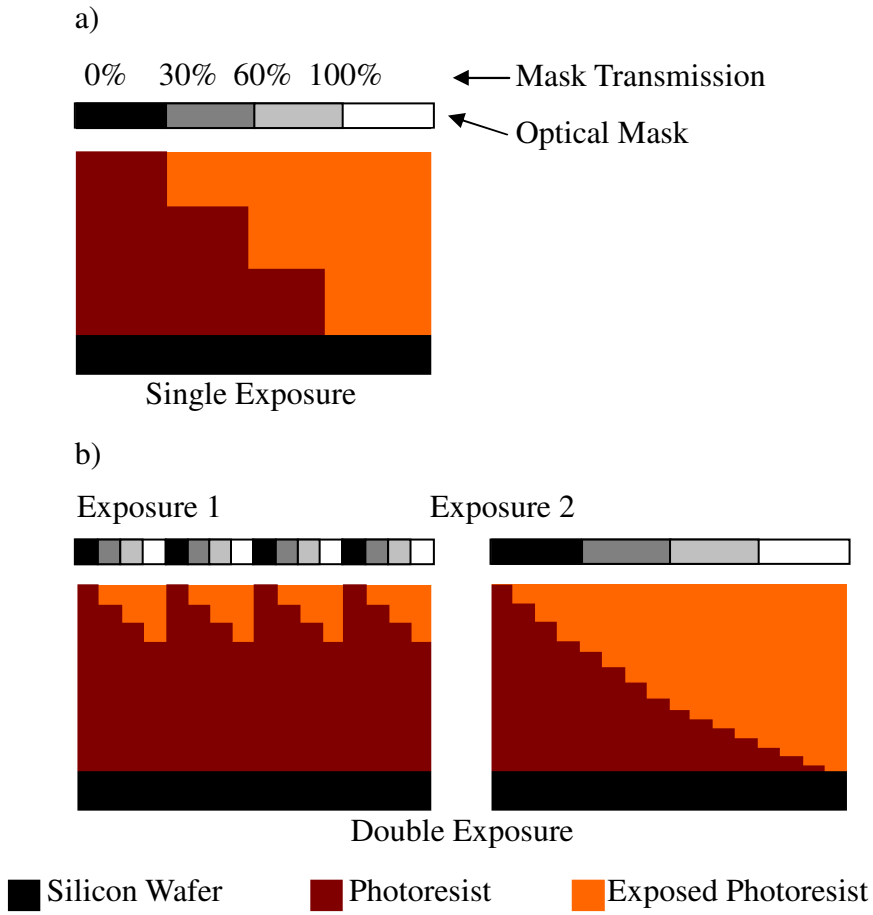

Figure 3.1: (a) A single gray-scale exposure produces four gray levels, while (b) double-exposure produces sixteen using the same set of four pixel sizes. The pixel size is represented by shades of gray on the optical mask.

Two overlaid gray-scale exposures will result in a gray level that is unobtainable by a single pixelated mask under the same processing conditions. Strictly speaking, it is possible for a pixelated mask to produce any gray level height by controlling the exposure time and development time. As described in

Sections 2.2.2 and 2.2.3, these processing variables may be specified to adjust the height of a given pixel size. However, once optimized processing parameters have been selected, a single-exposure pattern is limited to the number of gray-levels available by the mask fabrication process and the resolution of the projection photolithography system. Double-exposure alleviates this restriction because the combination of two exposures results in dose values that are in between doses produced during a single exposure. Every specific gray-scale dose used in the first exposure can be followed by any dose in the second exposure. An example mask utilizes three pixel sizes: one, two and three. If an area of photoresist is exposed with pixel size one for the first exposure, it may be exposed with pixel sizes one, two or three for the next exposure. The same is true if pixel size two or three were exposed first. Therefore, a total of nine combinations exist. In general, this means that the double-exposure technique will square the number of available pixel sizes with only one additional step to the gray-scale process (Figure 3.2).

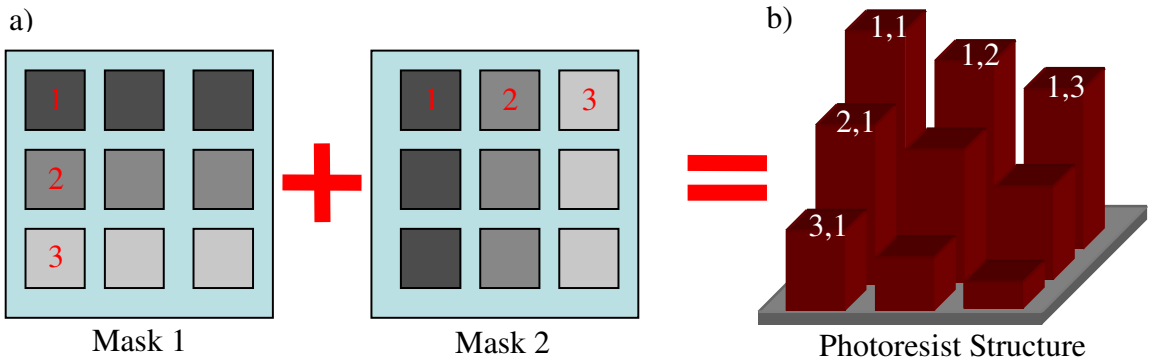

Figure 3.2: (a) Top-down view of two masks in an example double-exposure gray-scale process. The masks contain three pixel sizes. (b) Exposing each mask in turn produces the photoresist structure shown in oblique view. The masks contain n = 3 pixel sizes, so double-exposure yields n^2 = 9 gray levels.

In principal, any number of exposures can be overlaid in order to precisely control the total combined dose. Therefore, the total number of gray levels, l, is a function of the number of exposures, e, and the number of different pixel sizes, n:

$$l = n^e . \tag{3.1}$$

Multiple-step photolithography uses binary-exposure masks and a variable number of exposures, so Equation 3.1 becomes:

$$l = 2^e . \tag{3.2}$$

Although this equation shows that the number of levels increases quickly with increased exposures, alignment tolerances become prohibitive after only a few exposures. Also, overlaid exposures have not been demonstrated in the literature, reducing this to just n+1 levels. Double-exposure photolithography uses only two exposures to minimize alignment tolerances, but a variable number of pixel sizes:

$$l = n^2 . \tag{3.3}$$

In general, any number of masks could be used with this photolithography technique, but two exposures are sufficient for most applications.

This chapter describes the method and execution of double-exposure photolithography to fabricate 3D photoresist structures with a high vertical resolution. The calibration procedure is presented, along with design parameters unique to double-exposure gray-scale photolithography. Data collection methods are discussed and the calibration curve for mask designs is provided. Finally, the mask design procedure and final mask layout are presented.

3.2 Empirical Data Collection

Double-exposure gray-scale photolithography is calibrated by determining the experimental relationship between the relative gray-scale dose and the photoresist height. Empirical data were collected by exposing a test mask containing a calibration structure. Photoresist was deposited on a wafer and exposed to the calibration mask. After development, the resulting 3D profiles were measured using a stylus profilometer.

3.2.1 Calibration Structure

The calibration structure was designed on a test mask to provide a means to measure the gray level heights resulting from all pixel size combinations. The structure contained a grid of test pads, which are 100 μm squares of the same pixel size. The pads were arranged in an 8 x 8 pattern similar to the grid shown in Figure

3.2, which overlaps all combinations of pixel sizes using double-exposure photolithography. This grid used pixel sizes of 0.0, 0.8, 1.0, 1.2, 1.4, 1.6, 1.8 and 2.6 µm. The 0.0 µm and 2.6 µm pixels are simply transparent and opaque pads, respectively. Both exposures were physically located on the same mask. The first pattern was placed on the bottom left, and the second exposure pattern on the upper right corner, rotated by 90°. When the mask was rotated 180°, the exposures line up as shown in Figure 3.3.

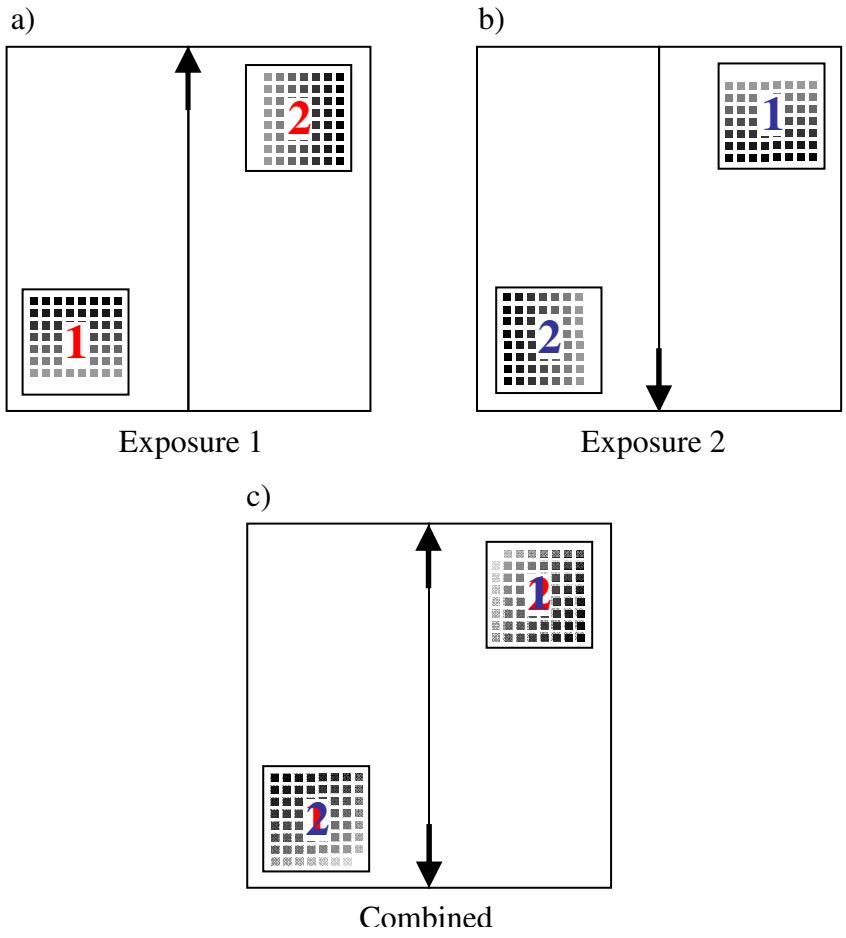

Figure 3.3: Top view of calibration grids on the test mask. (a) During the first exposure grid 1 is in the lower left corner. (b) The mask is then rotated 180 degrees for the second exposure. (c) The resulting combined exposure produces two calibration grids.

3.2.2 Photolithography Procedure

The double-exposure photolithography procedure is very similar to single-exposure photolithography or to any other projection photolithography process. A 6 µm layer of AZ9245 photoresist was spun onto a 150 mm silicon wafer in a Karl Suss ACS200 automated spin coating and developer tool. In this process, the wafer was vapor primed with a hexamethyldisilazane (HMDS) adhesion promoter. AZ9245 was deposited and the wafer was spun at 3000 RPM for 40 seconds. Finally, the wafer was soft baked on a hot plate for 90 seconds.

3.2.2.1 Wafer Cleaning

The purity of the wafer surface before depositing photoresist is critical for gray-scale photolithography. Contaminants that affect the photoresist spin generally produce a visible "swirl" pattern caused by inconsistencies in within the photoresist layer that usually lead to slightly different development rates on the same wafer. These swirl patterns are not usually an issue for planar photolithography with MEMS because the consistency within photoresist is not important. However, with gray-scale photolithography, any interior inconsistencies in the photoresist layer become undesirable patterns in the 3D structure. To avoid these issues, the wafers were cleaned by submerging in a "piranha" solution of a 4:1 ratio of 30% hydrogen peroxide to 96% sulfuric acid for 10 minutes.

3.2.2.2 Exposure

The wafer was exposed with a GCA i-line projection photolithography stepper using the calibration mask. The tool stepped the mask pattern across the wafer in a 5 x 5 square grid for a total of 25 dies on each wafer. The total combined exposure time for each die was entered as 1.5 seconds, but the exposure times for each individual exposure varied freely between 0.1 s and 1.4 s. The three most common exposure time sets were 0.75 s, 1.0s and 1.25s for the first exposure followed by 0.75s, 0.5s and 0.25s for the second exposure, respectively. After the first exposure, the mask was removed and rotated 180°. The second exposure was aligned to the first using the latent image in the photoresist. When photoresist is exposed, but not developed, the pattern is faintly visible to the naked eye or under optical microscope and is termed the latent image. Longer or more intense exposures produce a more visible latent image. Therefore, the longest exposure time of the two exposures was always used first, so that the latent image was as firmly defined as possible.

3.2.2.3 Development

After exposure, the wafer was developed in a 4:1 solution of deionized water and AZ400K, which contains potassium hydroxide as the active compound. The exposure time was selected so the development time would be between 6 and 7 minutes. As with traditional photolithography, a die is considered developed when

all the fully exposed photoresist (i.e. the mask transmission was 100%) is completely removed. The photoresist layer is never perfectly uniform across the wafer, so some dies often develop earlier than others. With planar photolithography, the wafer is simply held in the developer until all dies are completely developed. However, because gray-scale structures are much more sensitive to overdevelopment, as outlined in Section 2.2.3, the wafer must be removed before all dies are completely developed. Therefore, the wafer would be removed when about 70% of the dies had completely developed, producing a wafer with about 20% overdevelopment, 30% underdevelopment and 50% developed properly. While wafer-level yield is poor, the wafer can be cleaved prior to development to separate each die. Then each die can be developed individually, which greatly improves yield, but sacrifices processing speed.

3.2.3 Test Structure Measurement

The combination of both exposures in the test structure resulted in 64 double-exposure gray levels. After exposure and development, a Veeco Dektak 6M stylus profilometer was used to measure the height of each test pad. The profilometer scanned across each row of the calibration structure to measure eight gray levels at a time. The height of each level was measured individually using the profilometer software and recorded manually in a spreadsheet. The pixel sizes used for each test pad must be known to calculate the relative dose. The value of the pixel size was written on the calibration grid at the end of each row for the first

exposure and the end of each column for the second exposure. Therefore, the pixel sizes of a given test pad is listed at the end of its corresponding row and column.

3.3 Exposure Commutability

Multiple-step photolithography has been demonstrated with binary masks, but no previously reported results reported have shown the effect of overlaying multiple gray-scale exposures. Therefore, it is important to re-examine the exposure kinematics and any possible effect on double-exposure photolithography. As shown in Equation 3.4 (previously given in Chapter 1), the UV light intensity changes as a function of depth, z, and the absorption coefficient, α, as described in [38]:

$$I(z) = I_s \exp(-\alpha \cdot z) . \tag{3.4}$$

The absorption coefficient is given by:

$$\alpha = A \cdot \exp(-C \cdot dose) + B . \tag{3.5}$$

However, if the photoresist is unexposed (dose is zero):

$$\alpha = A + B . \tag{3.6}$$

A, B, and C are the Dill parameters of the photoresist [43]. These equations show that the exposure changes the properties of the photoresist. Specifically, the photoresist becomes easier to penetrate as it is exposed. This phenomenon occurs during any exposure, but is likely included in the calibration between the exposure dose and the photoresist height. However, this effect may have a greater impact on double-exposure photolithography, because the UV intensity changes during the course of the exposure. This raises the question of commutability between the two exposures. In other words, it is unknown if reversing the exposure order will produce the same gray level height, even though the total dose is the same.

This effect was simulated using Equations 3.4 and 3.5 with numerical methods. The photoresist exposure depth was calculated as a function of time using a given set of pixel sizes and exposure times. Then, the exposure was reversed and simulated again. In an example simulation, a pixel size of 1.0 μm was exposed for 0.5 s, followed by a 2.0 μm pixel exposed for 1.0 s. When this exposure combination was reversed, the difference between the final exposure depths was only 0.01 μm, showing that the exposure order commuted for this example (Figure 3.4). However, when the exposure times were doubled, the difference between the final exposure depths increased to 0.58 μm, which means the exposure order did not commute (Figure 3.5. Since the actual exposure time range used for this experiment is unknown due to issues with the projection photolithography tool, an experimental approach is required to determine if the exposure order will commute.

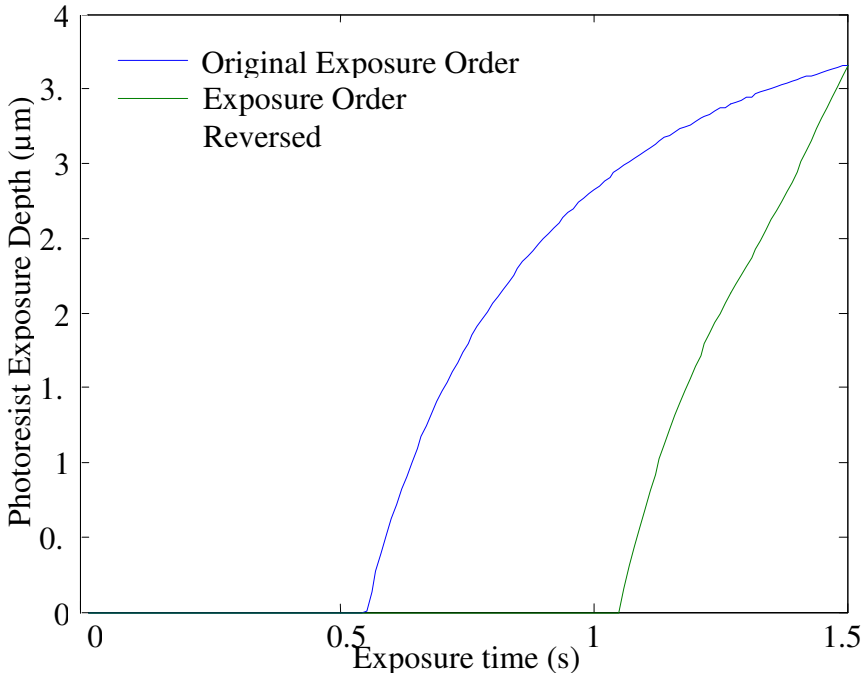

Figure 3.4: Graph showing the exposure depth into photoresist as a function of time for a double-exposure process. In this case, the exposures commute when the exposure order is reversed because the final photoresist exposure depth is the same.

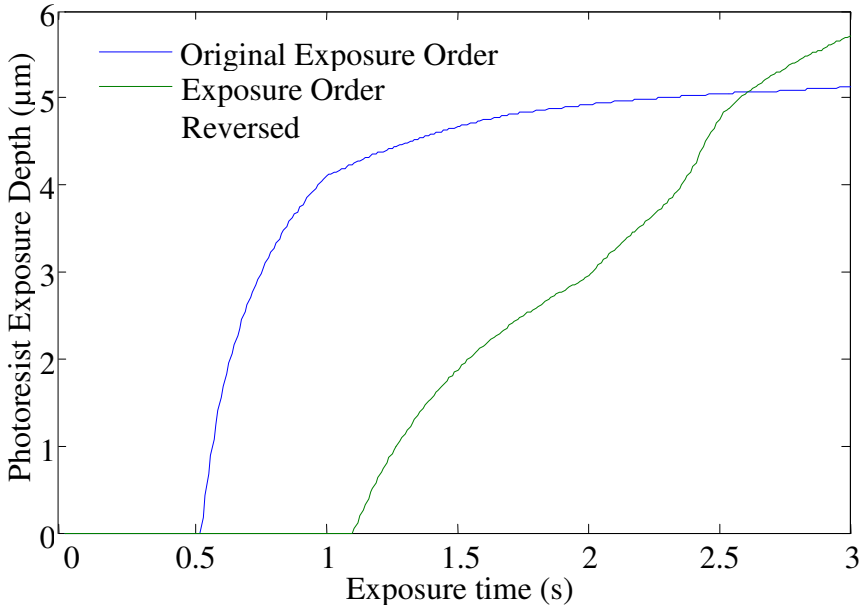

Figure 3.5: Graph showing the exposure depth into photoresist as a function of time for a double-exposure process. In this case, the exposures do not commute when the exposure order is reversed because the exposure time is longer than in Figure 3.4.

A simple experimental approach was utilized to test the commutability of the exposures within the typical dose range. The photoresist was exposed using the calibration mask with the same two exposure times. This created pairs of test pads that used the same two pixel sizes, but a different exposure order. Such pairs are termed symmetric pads. For example, a test pad exposed with a 1.0 μm pixel size followed by a 1.6 μm pixel size will have a pair that was exposed with the 1.6 μm pixel size first followed by the 1.0 μm pixel size. Since the exposure times are the same, the total dose is the same, but the doses for individual exposures are different. If the exposure times were not the same, no symmetric pads would be created. Symmetric pads across the calibration grid were measured and compared. The data strongly suggest that the exposures are indeed commutative. This is visually shown in Figure 3.6. Symmetric pixels on the calibration grid differed by an average of 1.5% of the total resist height, which is not significantly different from the average difference between gray levels formed by identical exposures. This clearly shows that the effect of the variation in the absorption coefficient from Equation 3.5 is negligible. This means that either the variation in the dose is low enough, or the dose values are all high enough to decrease the absorption coefficient by about the same value. While this result holds for the typical dose range used in these experiments, a different experimental procedure using a different photoresist, exposure time or even development time may produce exposure combinations that do not commute. Therefore, it is important to experimentally examine this effect before designing a double-exposure gray-scale mask.

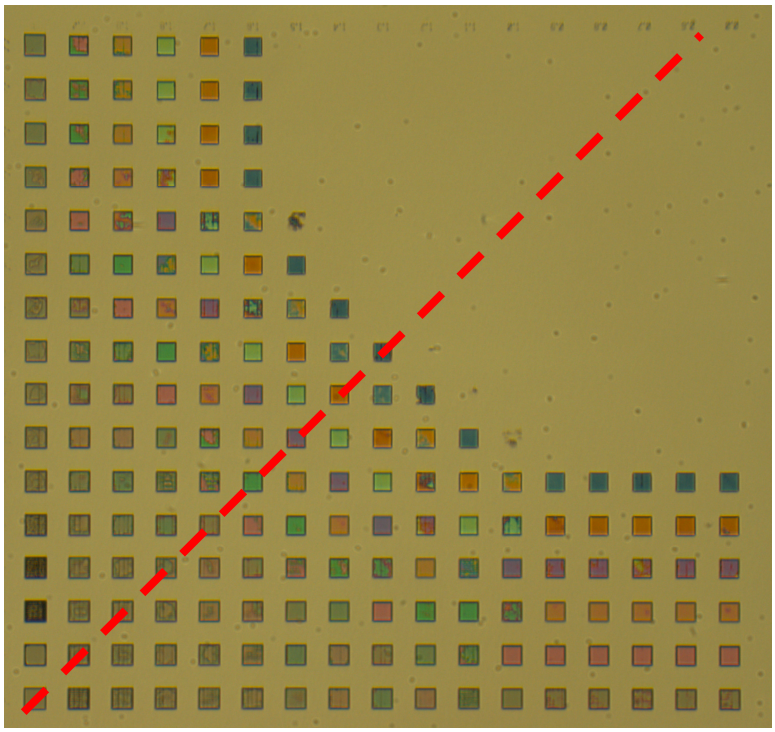

Figure 3.6: A micrograph of a calibration grid showing good symmetry. Gray levels are 100 µm on each side and the photoresist height is related to the color of the photoresist due to a filter effect. Gray levels across the line of symmetry, displayed as a broken red line, appear very similar in color, providing a qualitative estimate of commutability.

3.4 Calibration

Both single-exposure and double-exposure gray-scale photolithography processes require calibration in order to design a mask. Photoresist structures fabricated with single-exposure photolithography require a precise understanding of the dose applied and the height of the resulting gray levels. However, since the exposure and development parameters are held constant, the only variable controlling the dose is the pixel size on the mask. As described in Section 2.2.2, the

calibration involves finding a relationship between the pixel size and the gray level height. As shown in Figure 3.7a, one benefit of single-exposure photolithography is that the pixel order is logical; the pixels always increase in size for a decreasing profile. Calibration is only required to adjust the width of each gray level to match the desired profile shape, as shown in Figure 3.7b. Calibration is more complicated with double-exposure photolithography because the additional exposure step quadruples the number of dependent variables. The pixel order is not obvious, and moreover, is counterintuitive as shown in Figure 3.7c. Therefore, the first step to calibrating the double-exposure gray-scale process (Figure 3.7d) is to develop a method to calculate the applied dose.

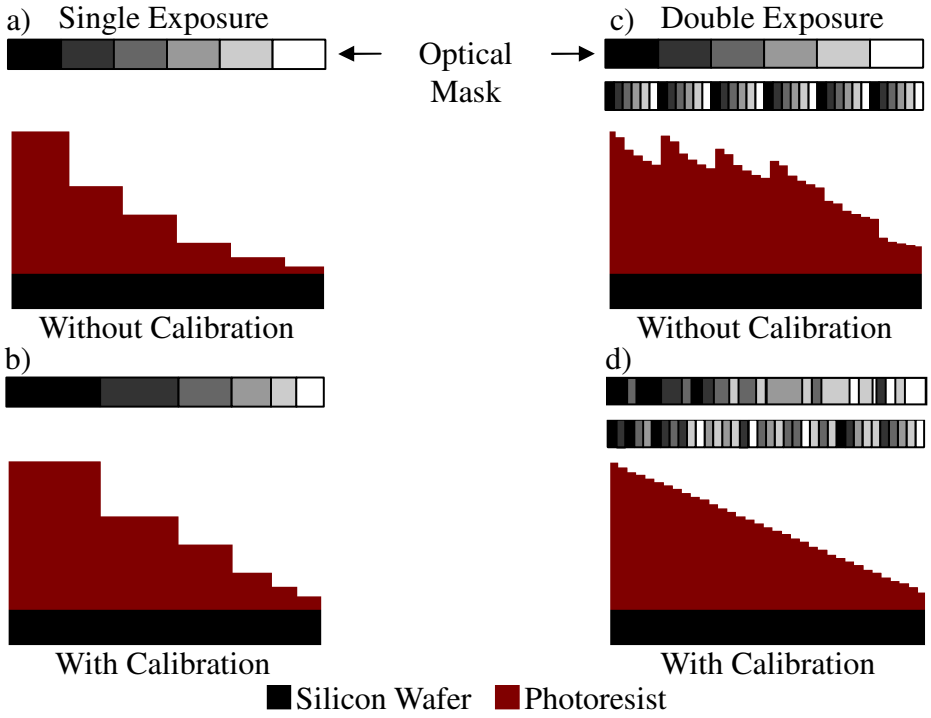

Figure 3.7: (a) The pixel order is clear in single-exposure, calibration is only required to determine the widths to realize a linear wedge as shown. (b) Both pixel order and width must both be determined when using double-exposure photolithography.

3.4.1 Double-Exposure Gray-Scale Dose

Calibration in single-exposure photolithography relates gray level heights to the normalized intensity given by Equation 2.5, which only depends on the pixel size. Using double-exposure photolithography, calibration requires a relationship between the gray scale height and the normalized dose. This function depends on the normalized intensity, I_n, for both exposures (Equation 2.5). As mentioned in Section 2.1.2, the projection photolithography tool scales the exposure time. Therefore, the selected exposure time is a unitless value normalized to an unknown exposure time standard, t_0. The normalize dose, d_n, is given by

$$d_n = \frac{I_s}{I_0 \cdot t_0} = I_{n1} \cdot t_{n1} + I_{n2} \cdot t_{n2} \,. \tag{3.7}$$

Here t_n is the normalized exposure time and the subscript *1* or *2* identifies the first or second exposure. The two doses for each exposure can be combined in a simple sum because, as proven in Section 3.3, the exposures commute for the range of doses used in these experiments. Comparing the normalized dose for double-exposure in Equation 3.4 to the normalized intensity in Equation 2.5 shows that the number of dependant variables increases from one to four.

3.4.2 Calibration Data Collection and Analysis

The data for exposure commutability were collected using the calibration structure described above. A second-generation calibration grid was created with more pixel sizes and was used for most of the calibration experiments. This grid was an identical design to the first structure, but used the 15 pixel sizes described in Section 2.4.1 along with a transparent and opaque level for a total of 17 different test pads. The 17 x 17 grid produced a total of 289 gray levels [44]. Again, calibration data were collected by stylus profilometry. The tool drags a stylus across the surface and measures the displacement of a needle as it passes over the structures. After the scan, the profile is leveled manually using points of known geometry. In typical operation, the heights along the profile are then directly measured by moving a software cursor. However, since each second-generation mask contained 289 gray levels, there are two calibration grids per die, and 25 die per wafer. This presents an unwieldy amount of data collection for even a single experiment.

To expedite the data collection process, the calibration structures were analyzed automatically using a computer program written for this purpose. This program was written in a computer language similar to MATLAB, called Octave. After a row of calibration structures were scanned in the profilometer and the data were leveled, the scan data (Figure 3.8) were saved in a comma separated variable (CSV) file for further analysis.

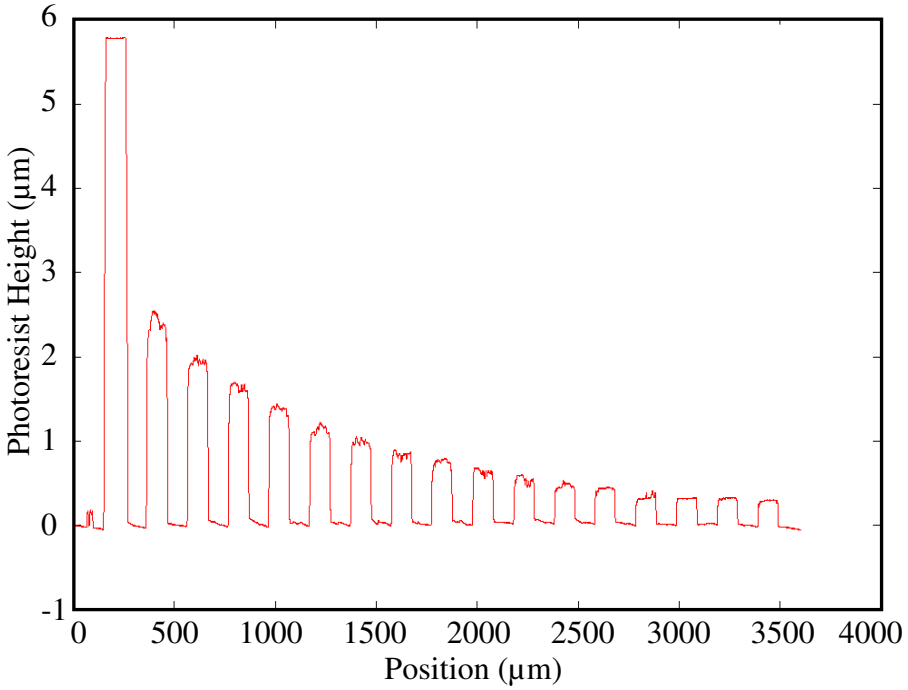

Figure 3.8: Example stylus profilometer scan along a row of the calibration grid. Each gray level is automatically detected, identified, and measured by the analysis program.

The seventeen files for each grid were saved in the same folder with file and folder names that contained the pixel size, exposure times and die number of the sample. The pixel size given in each filename was the pixel size of the first exposure for all test pads in that scan. The program would read each folder, parsing the filename information to automatically identify the exposure times and the row pixel size for each test pad. The program would then extract the gray level heights from each file and determine the column pixel sizes for each pad. This information was then used to calculate the normalized dose for the calibration curve.

The program processes each file using an analysis algorithm to identify each gray level in the scan. The first step is to isolate the gray level pad from the rest of the profile, as shown in Figure 3.9a. The test pad is isolated using an adaptive algorithm that detects the leading edge of the gray level by analyzing the slope. The length of each test pad is 100 µm, so the other edge of the isolation is selected 150 µm after the leading edge. Once the gray level is isolated, a random consensus algorithm [45] identifies the height of the gray level (Figure 3.9b). This algorithm was developed to filter out noise from surface data, which is applicable to this situation. Conceptually, this program finds the flattest point among the data and identifies this as the height of the gray level. The program then discards the current gray level and repeats this procedure for the next gray level in the scan file until no more gray levels are detected (Figure 3.9c).

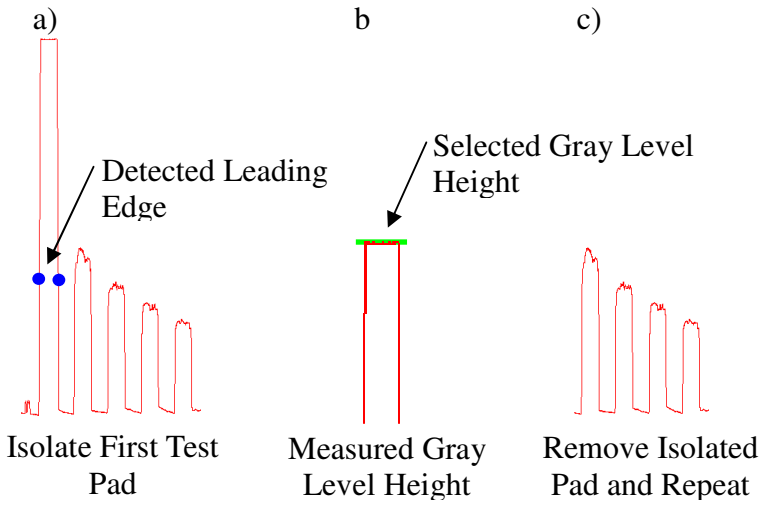

Figure 3.9: The analysis process for each scan: (a) Isolate the first test pad, (b) Measure the gray-level height of that pad, (c) Remove the pad and repeat the process.

The program then opens the next scan file and repeats the entire process. Once all gray levels have been processed in every file, the program calculates the relative dose for each measured gray level using Equation 3.4 and writes the data in a CSV file. The entire process takes less than a minute, compared to several hours when identifying gray levels manually using the profilometer software.

3.4.3 Calibration Curve

The CSV data were analyzed using a graphical analysis tool similar to Origin called QtiPlot. The normalized dose and corresponding photoresist height were analyzed in a scatter plot, as shown in Figure 3.10. In order to predict the photoresist height using a given dose, a relationship between these two values must

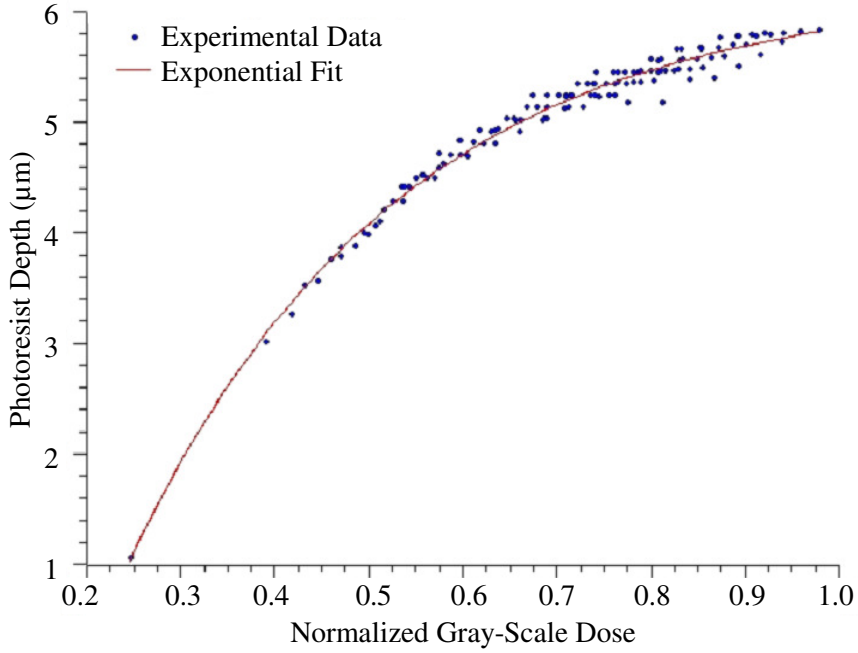

Figure 3.10: The calibration curve for double-exposure gray-scale photolithography. An exponential fit provides the empirical relationship between the dose and the height.

be established. The measured photoresist height was correlated with the calculated normalized dose for every pixel combination on the calibration grid. Due to the exponential nature of the exposure kinetics, the data were fit using a nonlinear least squares method to the exponential equation:

$$depth = y_0 + A \cdot [1 - \exp(-dose \cdot B)]. \tag{3.8}$$

As shown in Figure 3.10, this resulted in the following calibration curve

$$depth = -8.85 + 15.11 \cdot [1 - \exp(-dose \cdot 3.30)] \tag{3.9}$$

The above calibration can now be applied in conjunction with the relative dose given by Equation 3.7 to calculate the resulting exposure depth in photoresist for a given a set of pixel sizes and exposure times.

3.5 Exposure Ratio

To design a double-exposure mask for a 3D structure, the calibration curve requires both the pixel size and exposure time for both exposures. The pixel sizes will obviously vary across the mask, but the optimum exposure times must be determined. The total exposure time is generally selected for the photolithography process as described in Section 2.2.2, but the ratio between the two exposures can

be varied freely and must be optimized. The calibration grid was exposed to three different time ratios, 1:1, 1:2 and 1:5 as shown in Figure 3.11. It was observed that the exposure time ratio controlled the vertical distribution of gray levels throughout the photoresist height. In general, the optimum ratio between two exposures will produce an even distribution of gray levels throughout the photoresist, enabling smoother sidewalls. Mathematically, this means the average and maximum step size between gray levels is as small as possible. If an application required smoother sidewalls in only part of the photoresist, the exposure time could be optimized to focus more of the gray levels within this region. In Figure 3.11, most of the gray levels occur in the lower region of the photoresist because most of the pixel sizes transmit more than 50% of the incident intensity. While a ratio of 2:1 appears to be the best visually, a more analytical approach was used to select the final exposure times.

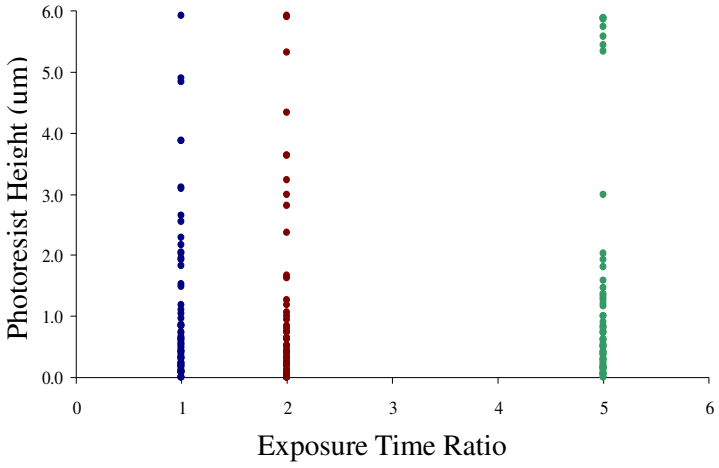

Figure 3.11: Different exposure time ratios produce a different vertical distribution of gray levels.

Optimization of the exposure time ratio would be slow using experimental methods because only one ratio can be tested at a time. To operate more efficiently, the calibration curve was used to simulate the average step height for a given exposure time ratio. A computer algorithm began with a ratio of 1:1 and calculated the normalized dose for every pixel combination. The normalized dose and the calibration curve were then used to calculate the resulting average step height. The exposure time ratio was then increased slightly, and the resulting effect on the average step height was observed. A simple minimum-finding algorithm was applied to find the exposure time ratio that produced the smallest average step height. The optimum exposure time ratio was calculated to be 1.78:1, which was used in for mask design and all subsequent exposures.

3.6 Mask Design

More than a million pixels must be precisely placed to design a pixelated gray-scale mask. Therefore, a series of computer programs were developed to assist in the mask design process. First the program discretized the desired structure onto a grid with the same spacing as the pixels on the mask. Next, the desired structure is approximating using the available gray levels for the selected process. These gray levels are then used to write out the mask layout file. This process, shown in Figure 3.12, will be described in more detail in the following subsections.

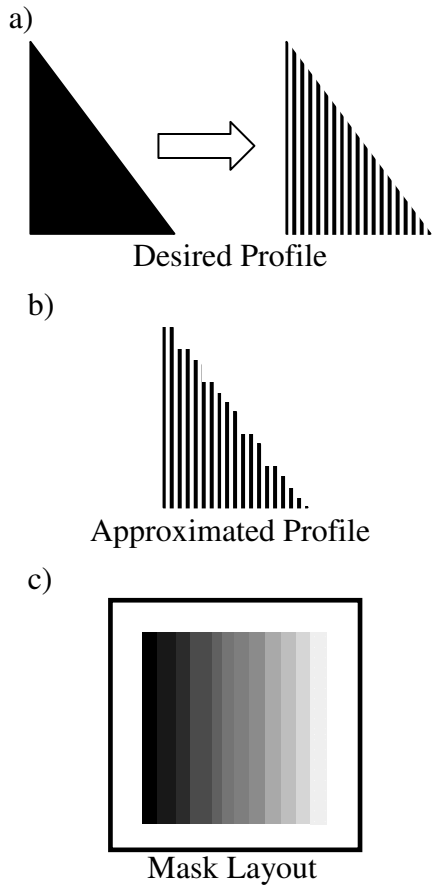

Figure 3.12: The mask process: (a) discretize the desired structure, (b) approximate the profile, and (c) write out the mask layout file.

3.6.1 Desired structure

In order to fabricate any arbitrary structure, the mask design program requires a description of the structure in (*x, y, z*) coordinates. Since initial structures are desired for a technology demonstration, simple geometries were selected that could be defined mathematically. Possible structures included basic shapes like wedges, bowls and domes. The specific dimensions, such as height, length and radius of these shapes were adjustable, so a variety of geometries could be

designed. Each shape was designed using a mathematical equation, which is continuous. However, the pixel structure on the mask is a discrete grid. Each desired geometry was discretized by interpolating the geometry onto a grid with the same spacing as the pixels (Figure 3.12a), which was termed a height-map.

Wedge structures were created by defining the x coordinates of each point, using the pixel spacing and the length of the wedge. Next, the height at each x coordinate was calculated using the linear equation for the wedge. No y coordinates were used because the one-dimensional structure could be repeated in the mask layout software to define the wedge width. All other structures were radial, but were defined similarly. First the x and y coordinates were defined for the first 45 degrees of the structure. Next, the radius at each x and y coordinate pair was calculated. Finally, the equation for the structure was used to calculate height at each grid point. Wedges, turbines and races were designed with a simple linear equation, while the bowls and domes were defined as an oblate spheroid using the following equation:

$$z = h \cdot \left(1 - \sqrt{1 - \frac{r^2}{R^2}} \right). \tag{3.10}$$

The structure height, z, is a function of the radius, r, and the constants h and R, which are the total height and radius of the device, respectively.

3.6.2 Height-list

The height-list is a lookup table that provides a link between the possible gray level heights and the corresponding pixel sizes to produce that gray level. When designing a mask, this allows a desired photoresist height to be matched to the closest available gray level and the corresponding pixel sizes. While the height-list is a fixed table, its values are generated using the calibration curve and are not fixed. The pixel spacing, exposure times and pixel limitations are provided at execution. The pixel size limitations include the minimum spot size and the address size. The available square pixel sizes are then calculated as described in Section 2.4.1. Once the list of pixel sizes is created, the program calculates the relative dose using Equation 3.7. Finally, the height-list is created using the calibration from Equation 3.9, which converts each relative dose into a height in photoresist. Specifically, the calibration curve converts the dose into a development depth, but translates this into the gray level height using the total photoresist thickness.

3.6.3 Pixel-map

The pixel-map contains two array structures that hold the pixel layout for the mask. This array is assembled using both the height-map and the height-list. The program cycles through each point on the height-map and finds the closest available gray level from the height-list. After repeating this process for all points on the height-map, the desired structure can now be expressed in terms of the available

heights (Figure 3.12b). Each available height is linked to a corresponding set of pixel sizes, so it is now possible to write out the pixel structure.

3.6.4 Mask Creation

Once a pixel map is created for a desired structure, the program writes out this information in a set of command files, one for each exposure, which is readable by Tanner L-Edit layout software. As a command file is executed, the pixels for the desired structure are automatically placed in a cell. After all desired structures have been created and read into L-Edit, the mask is assembled by arranging these cells into a master cell. To be cost effective, both exposures were positioned on the same mask, similar to the calibration grid. The first exposure design is located on the left half of the mask, and the corresponding second exposure is flipped and inverted on the right half of the mask.

For these experiments, a variety of wedge, bowl and dome structures were placed on a test mask. These structures were selected to demonstrate the double-exposure photolithography process. Wedges were designed with various lengths and heights and bowl and dome structures were created with various heights and radii. Most structures were fabricated using all 15 pixel sizes and the opaque and transparent exposures. However, but some “gray-scale only” structures were also fabricated using only the 15 gray-scale pixels. The primary mask structure is shown in Figure 3.13.

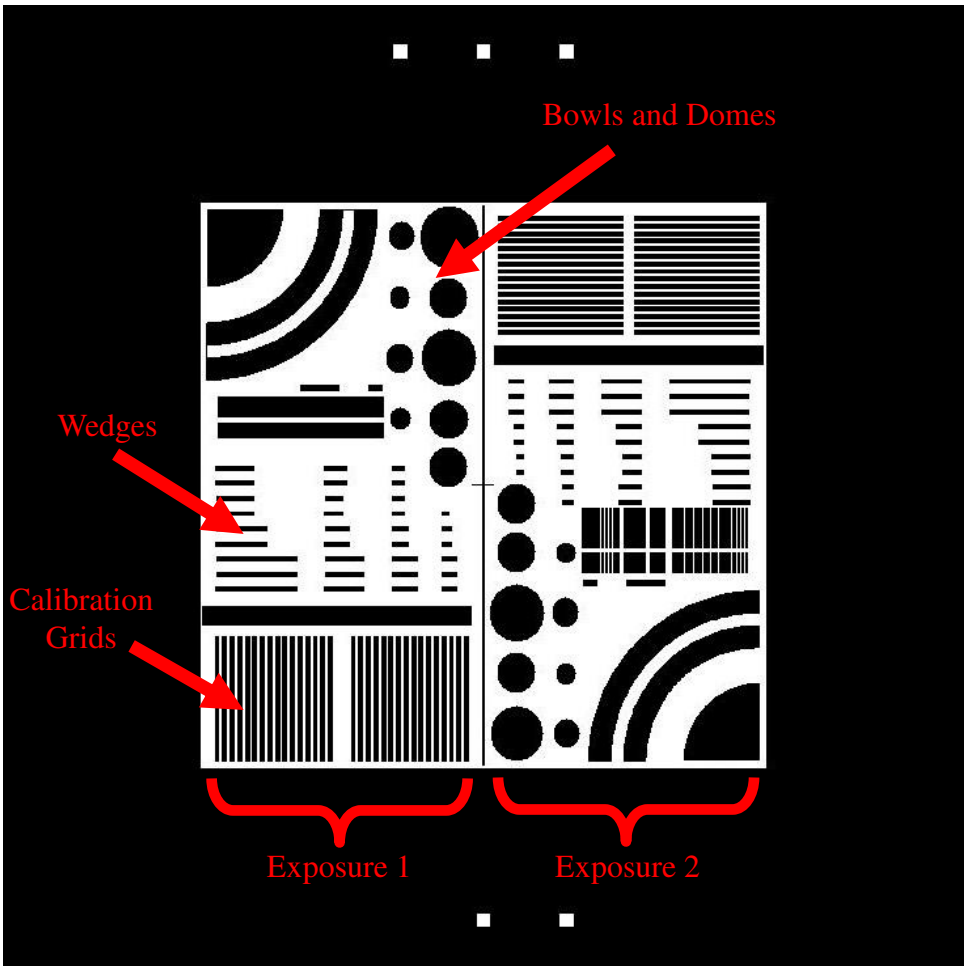

Figure 3.13: The mask layout contains both exposures on a single mask. Individually pixels are invisible, but the designed structures are roughly outlined.

Chapter 4

Fabrication of 3D Structures

4.1 Introduction

Upon completion the test mask, the first 3D structures were fabricated using double-exposure gray-scale photolithography, showing a clear improvement in the vertical resolution. This chapter presents a quantitative and qualitative assessment of this improvement as compared to single-exposure photolithography. In addition, this chapter describes designed photoresist structures measured by profilometer and scanning electron microscope (SEM). Some observed issues with this technology are discussed, including misalignment between the two exposures and the inclusion of opaque features in the double-exposure process.

4.2 Improved Vertical Resolution

The improved vertical resolution achieved with double-exposure gray-scale photolithography enables realization of structures that were never possible using pixelated gray-scale technology. Using the same set of seventeen pixel sizes, with

the same exposure and development procedure, double-exposure photolithography produced 289 gray levels compared to seventeen gray levels using a single exposure. Double-exposure photolithography decreased the average step height 0.19 μm to 0.02 μm and the maximum step height decreased from 0.43 μm to 0.2 μm. This is an order of magnitude improvement in the average step height and halves the maximum step height.

By implementing double-exposure photolithography, the accuracy of fabricated structures to the desired profile is increased compared to structures fabricated with single-exposure photolithography. To illustrate this point, a wedge structure was fabricated using both photolithography techniques is shown in Figure 4.1. To ensure comparability between the two wedges, the "single-exposure" wedge was actually fabricated on the same wafer as the double-exposure wedge. However, the mask pattern for this wedge was the same for both exposures, making it identical to a true single-exposure wedge. Individual gray level steps are clearly visible in the single-exposure profile, while the double-exposure profile has a much more continuous profile. The average difference between the fabricated structure and the ideal wedge profile was 0.98μm (33% of structure height) using single-exposure gray-scale and 0.17μm (6% of structure height) using double-exposure gray-scale photolithography. It is important to note, however, that roughness is more extreme in the double-exposure structure, which will be discussed in later sections.

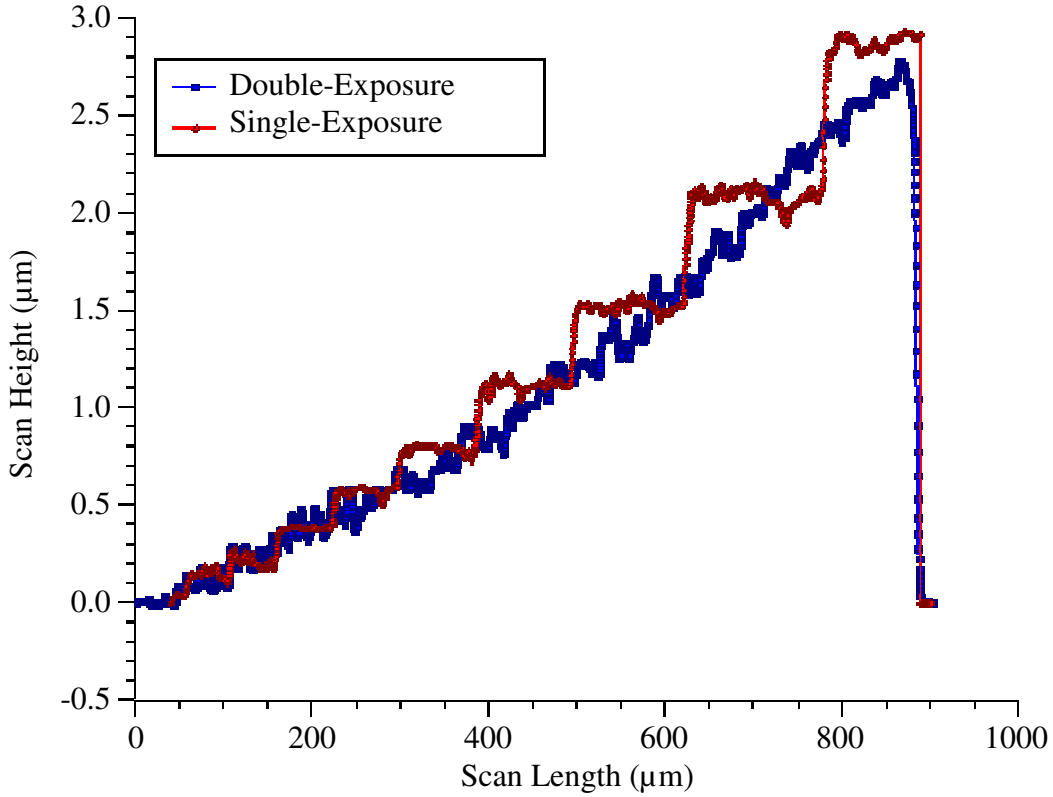

Figure 4.1: Profilometer scan of single-exposure and double-exposure photolithography structures. The double-exposure structure shows more roughness, but matches the desired wedge structure more closely overall.

This improvement in vertical resolution can be observed qualitatively by examining SEMs of the two wedge structures. Figure 4.2 is an SEM from a 35 µm segment of a wedge structure fabricated with single-exposure photolithography. Within this region, three distinct gray levels are visible, as annotated with a red dotted line. The overall structure is smooth, but each step height is clearly pronounced.

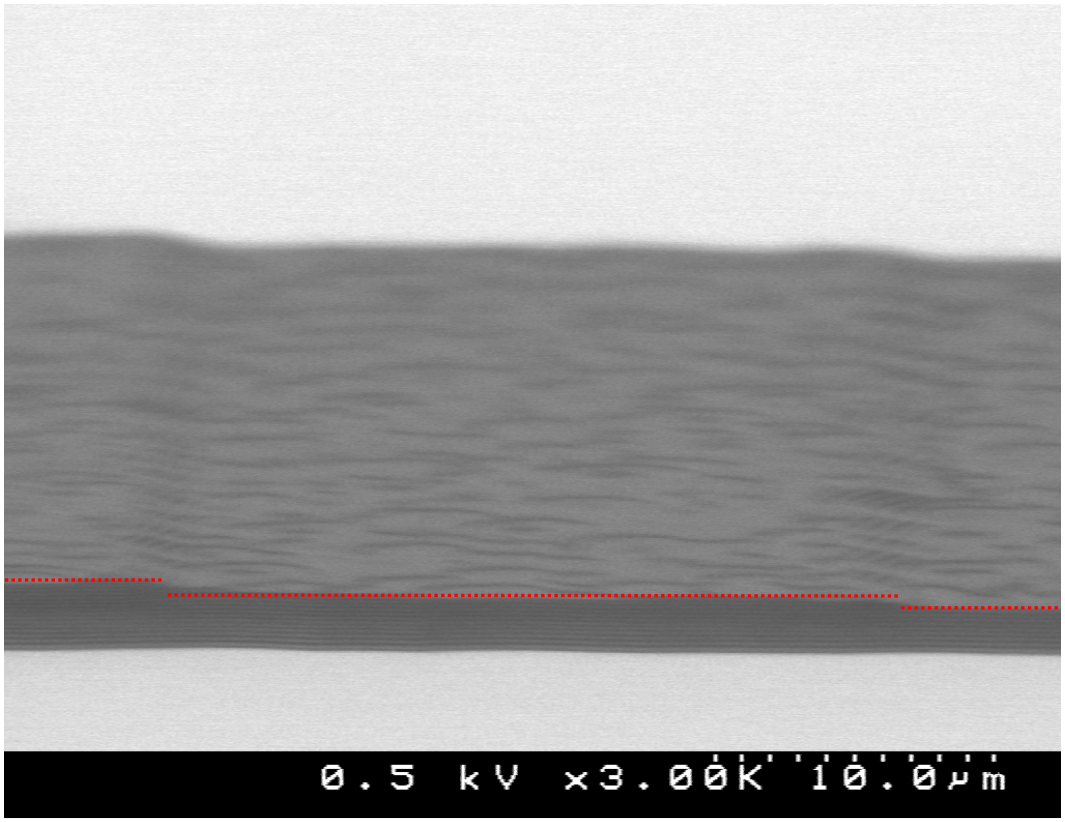

Figure 4.2: SEM micrograph of a portion of a single-exposure wedge structure. Three individual gray levels are visible, outlined with a red dotted line.

A similar SEM was taken of a double-exposure wedge on the same wafer as shown in Figure 4.3. Five gray levels are clearly visible in the same region, and the step size appears to be smaller than the steps in the single-exposure wedge. However, some of the boundaries between gray levels, especially the leftmost, appear to have a "bump", which is not present in the single-exposure structure. This effect may be caused by a slight misalignment between the two exposures, which will be discussed in the Section 4.4.

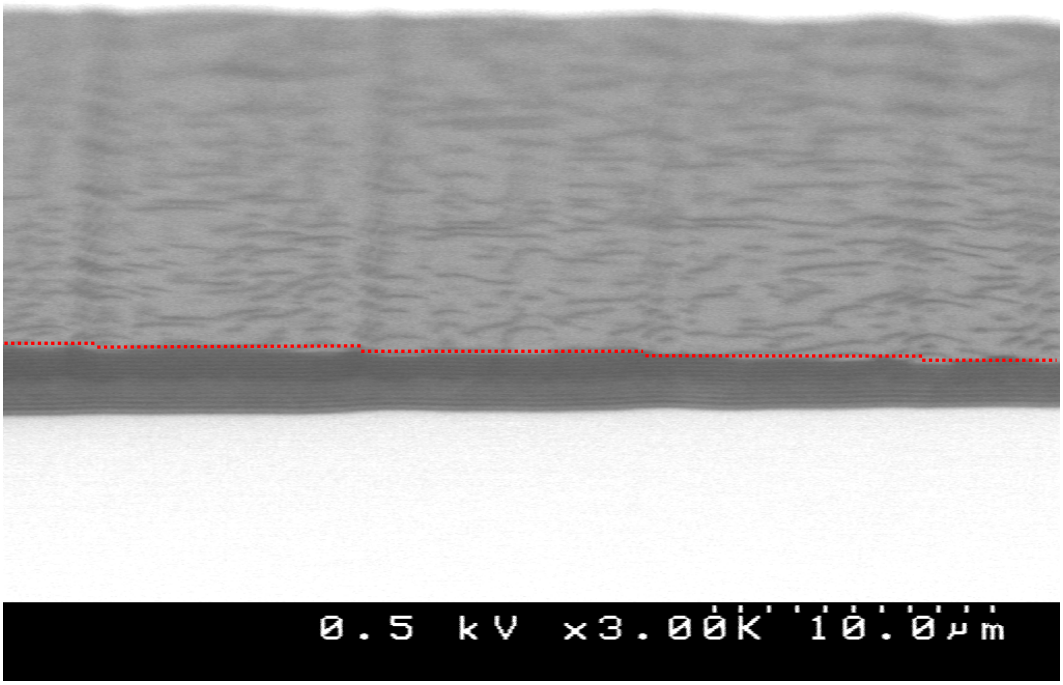

Figure 4.3: SEM micrograph of a portion of a double-exposure wedge structure. Each gray level is outlined by a red dotted line.

4.3 Designed Structures

Several types of structures were designed and fabricated using double-exposure gray-scale photolithography. Most of these structures utilized all seventeen pixel sizes, which creates gray levels through the entire photoresist. However, some of the wedge and dome structures used only the fifteen gray-scale pixels, which do not include the 2.6 µm opaque exposure and the 0.0 µm

transparent exposure. These structures were referred to as "gray-scale-only" because every location on the structure was created using a gray-scale pixel. Unfortunately, structures fabricated using all seventeen pixel sizes did not match the designed profile, because of the opaque pixels. Only the regions using gray-scale pixels matched the profile. Fortunately, this means that the gray-scale-only structures matched the desired profiles very well. For example, the wedge (Figure 4.4) and bowl profiles (Figure 4.5) closely match the desired profile. Even though roughness is present, it is smaller than the step height would be if the profile were fabricated using single-exposure photolithography.

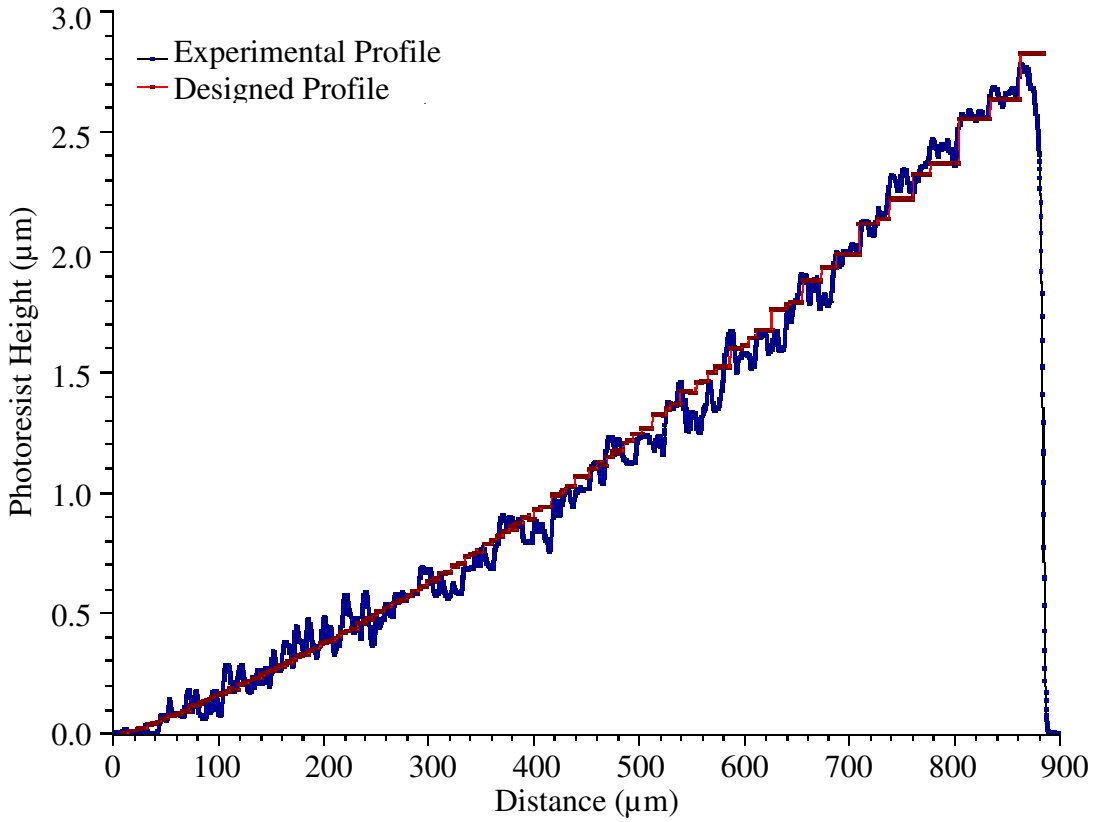

Figure 4.4: Profilometer scan of a double-exposure wedge compared with the designed profile. The experimental profile shows a high degree of roughness.

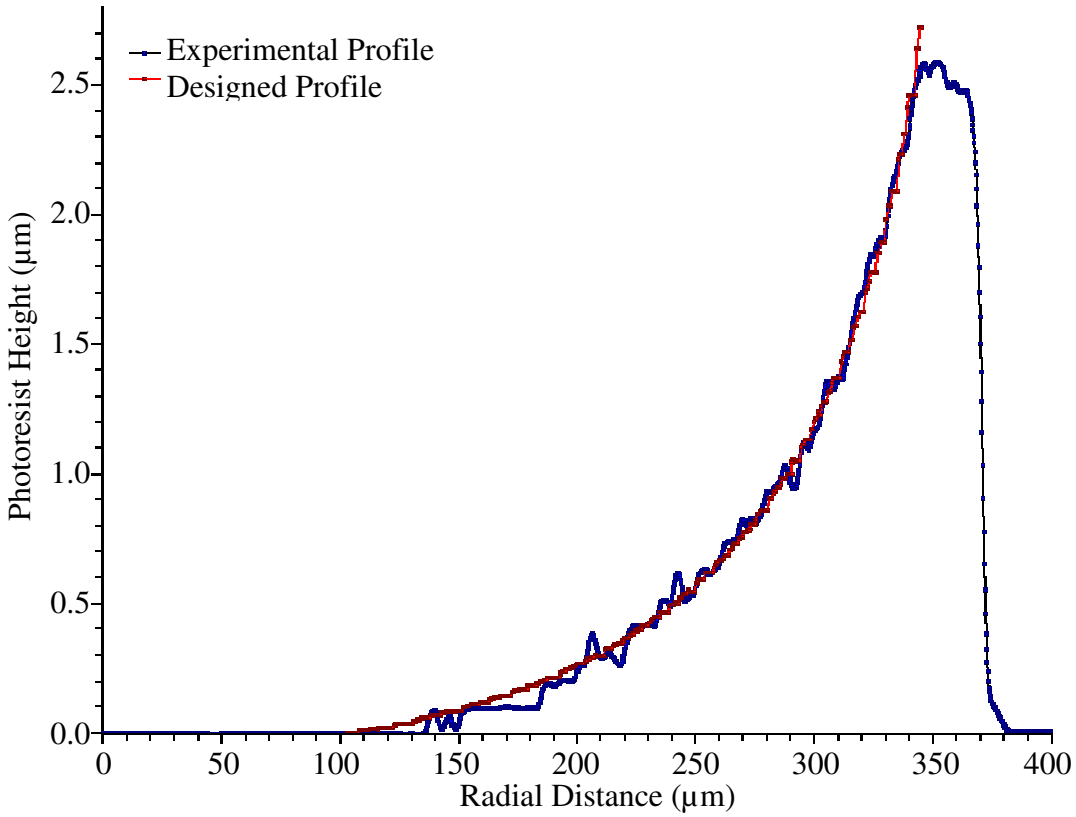

Figure 4.5: Profilometer scan of a double-exposure bowl structure compared with the designed profile. Slopes show less roughness than the wedge structure.

SEM micrographs of these structures show similar qualitative results. A comparison between a single-exposure wedge (Figure 4.6) and a double-exposure wedge (Figure 4.7) shows that the double-exposure wedge has a much gentler slope over the entire profile, but contains several pronounced "bumps" along the slope. Additionally, the SEM of a bowl structure (Figure 4.8) shows less overall roughness, buts several points of higher roughness, similar to Figure 4.5.

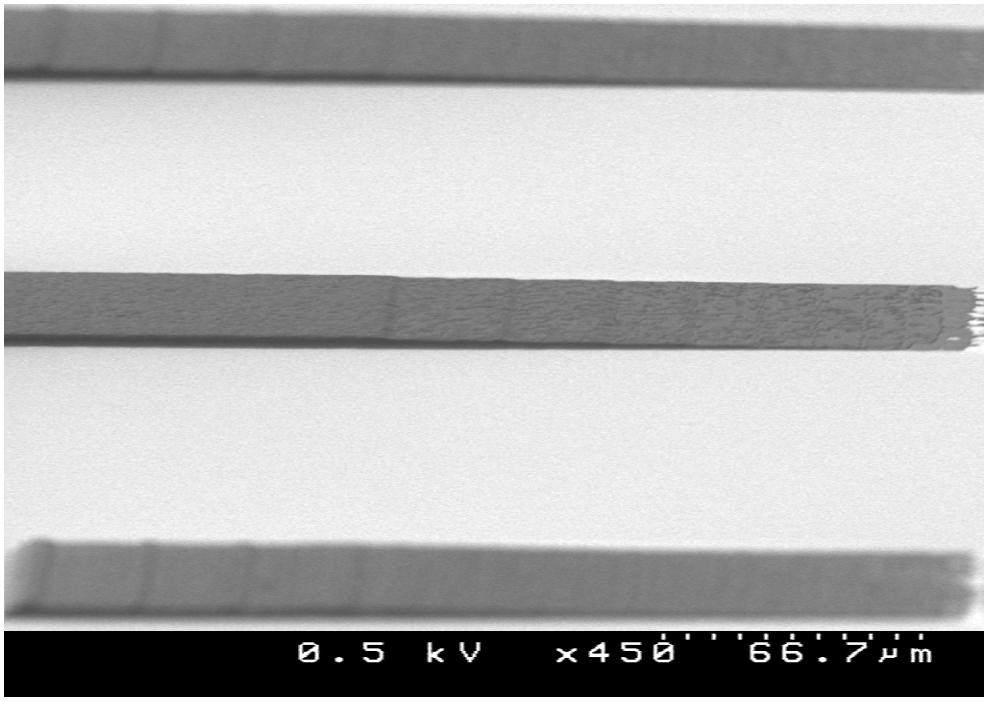

Figure 4.6: SEM of entire single-exposure wedge structure (middle wedge). Several larger gray level steps are clearly visible.

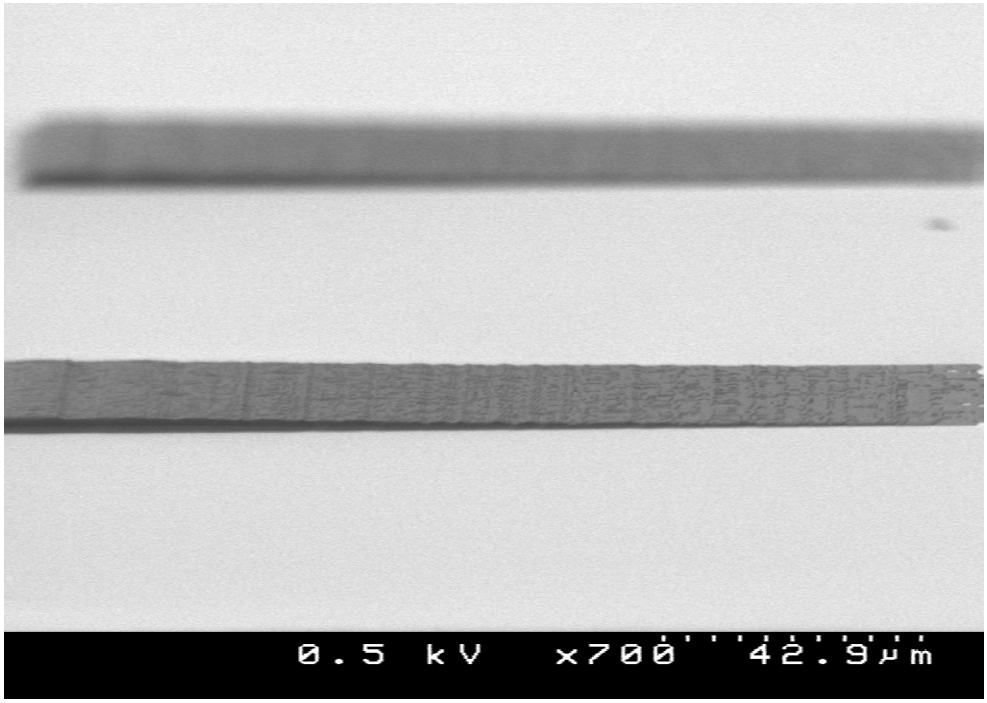

Figure 4.7: SEM of entire double-exposure wedge structure. The overall wedge profile is smoother than the single-exposure wedge, but several larger bumps are visible within the profile.

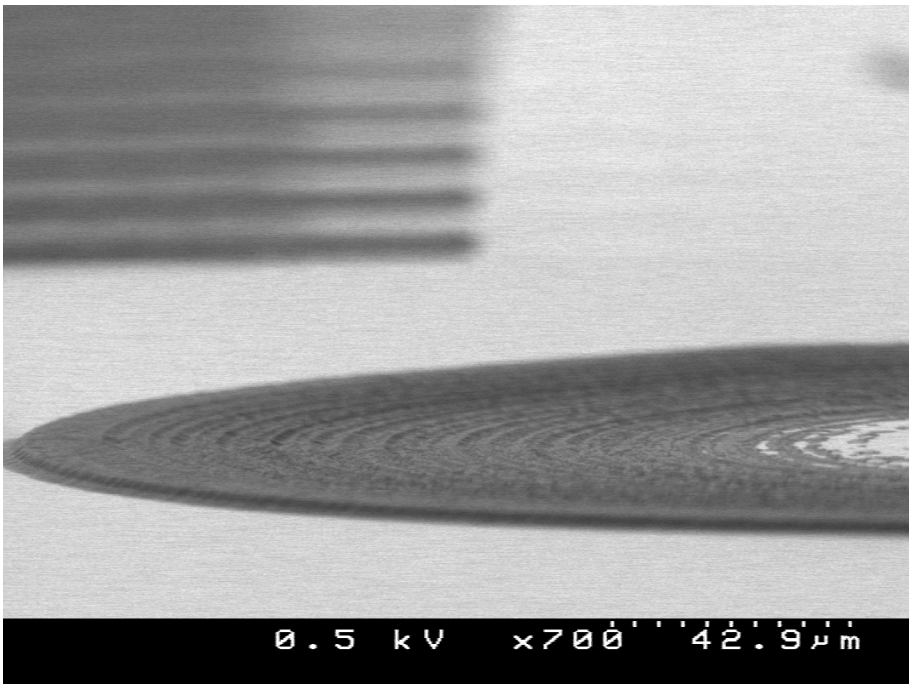

Figure 4.8: SEM of a double-exposure bowl structure with an inwardly-sloping profile.

4.4 Mask Misalignment

The double-exposure profile shown in Figures 4.1 is closer to the designed structure than the single-exposure profile even though it exhibits a larger degree of roughness. To explore the cause of this roughness, the effect of misalignment between the two exposures was investigated (Figure 4.9). If the second exposure is misaligned from the first exposure, erroneous pixel combinations will be exposed at the gray level boundaries [46]. These erroneous pixel combinations are outlined by gray dashed lines. In Figure 4.9b, the photoresist exposes deeper because the

misaligned region is more transparent than the intended design and in 4.9c the case is reversed.

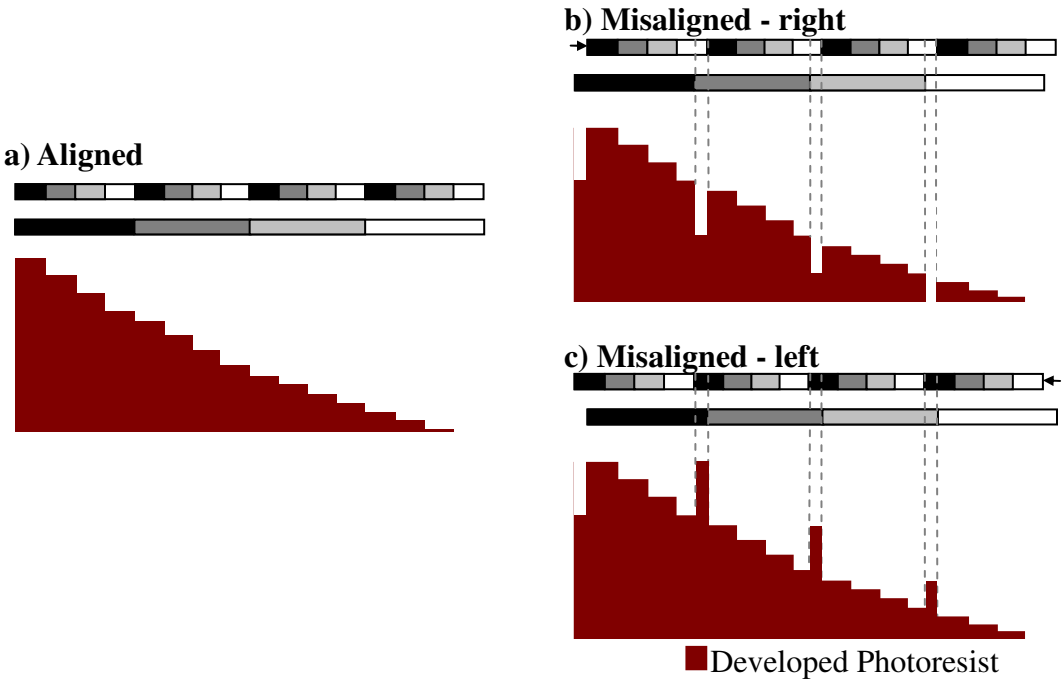

Figure 4.9: (a) An example double-exposure profile when the two masks are aligned as designed. (b) If the mask is misaligned to the right, overlap causes overexposure, producing valleys. (c) If the mask is misaligned to the left, overlap causes underexposure that produces peaks.

Drastic misalignment can be seen clearly on using an optical microscope but, smaller misalignments that are harder to detect visually even though they are clearly visible in a profile. For example, large spikes in the profile shown in Figure 4.10 signify that the mask was misaligned. However, the lower region of the wedge profile also shows an increased degree of roughness compared to structures in Figures 4.4 and 4.5, which contain no obvious signs of misalignment. This suggests that misalignment can cause increased roughness in a double-exposure profile.

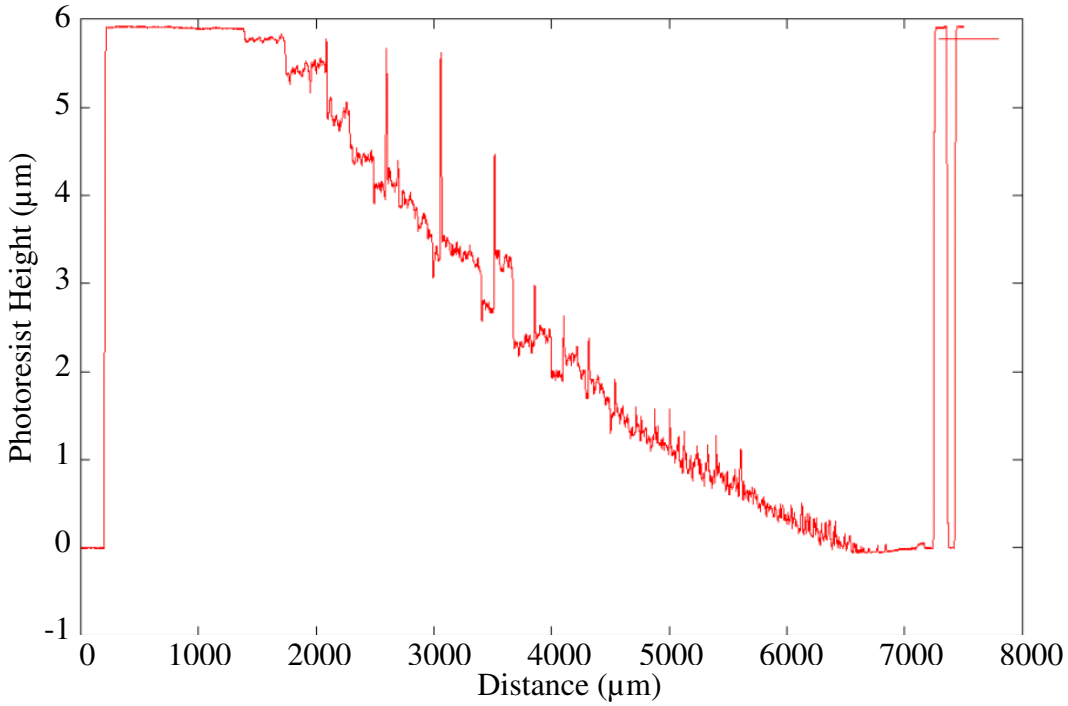

Figure 4.10: Stylus profilometer scan of a wedge profile showing very bad misalignment. It is interesting to note that the presence of the very large spikes is accompanied by increased roughness in the lower region of the photoresist compared to Figure 4.1.

4.4.1 Tolerance for Misalignment

In order to investigate the source of this effect, misalignments of 0.1 µm and 0.2 µm were simulated using the calibration curve on a previously designed wedge structure. The calibration curve was used to simulate the effect of exposing previously designed mask layouts with no misalignment. The pixels for each exposure were read into an analysis program and the dose at each location was calculated. Next, the calibration curve was applied to convert each dose into a predicted photoresist height. Then the second mask was shifted and the process was

repeated to simulate the effect of mask misalignment. However, since the misalignment is less than the 2.6 μm pixel spacing, diffraction was approximated by interpolating the calculated dose between the pixels at a 0.1 μm grid spacing. The second mask was then shifted and the two doses were calculated at each grid point. The data spacing was restored by averaging the interpolated grid points. After calculating the misaligned dose profile, the calibration curve was used to calculate the predicted photoresist height in the presence of mask misalignment.

The calculated misalignment exhibits an increased roughness with increasing misalignment, as predicted (Figure 4.11). The degree of roughness is also consistent with the experimental results shown in Figure 4.1. Logically, a larger deviation from the designed structure occurs if the adjacent pixels across the misaligned boundary differ greatly in size. Simulation shows that it would be possible to reduce this effect by removing certain gray levels with a large difference in adjacent pixel size. Experimentation with the misalignment simulation showed that if all adjacent pixel sizes differ by less than 0.7 μm, the roughness will be reduced to be on the order of the average step height. This new design rule was implemented into the mask design algorithms and a wedge structure was designed and simulated using this new rule. The results, shown in Figure 4.12, show a dramatic reduction in roughness, even under some misalignment. By choosing to remove the appropriate pixels, it is possible to minimize the effect of misalignment.

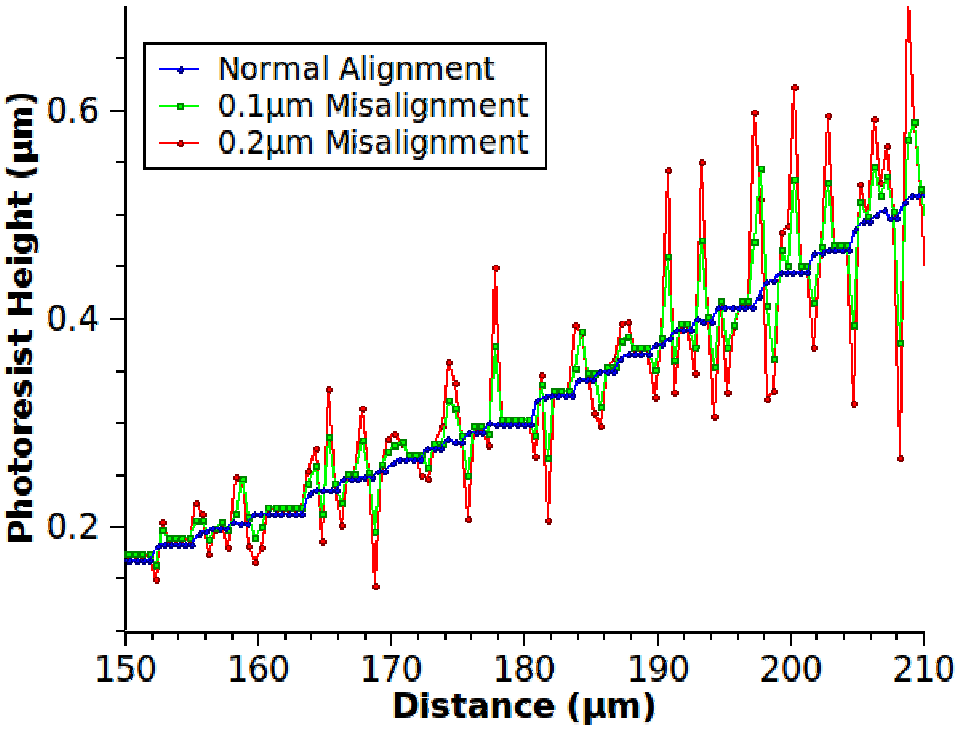

Figure 4.11: Simulated profile showing increased roughness with increased misalignment.

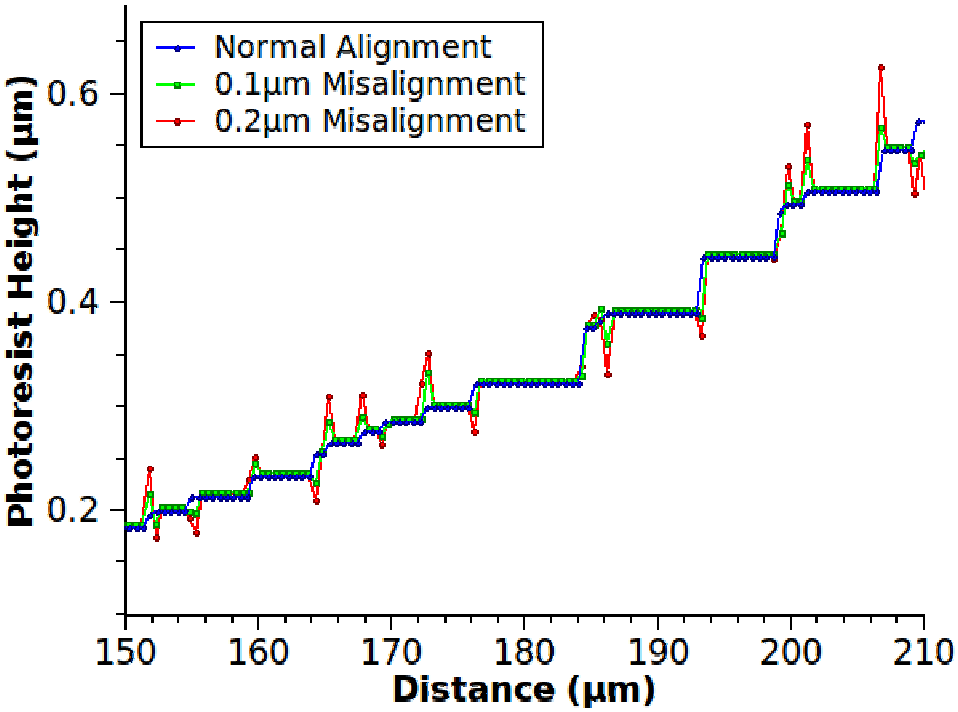

Figure 4.12: Simulated profile after applying the design rule to the simulation, demonstrating fewer irregularities at the expense of vertical resolution.

4.5 Opaque Levels

Another observed issue with double-exposure gray-scale photolithography was using structures designed with opaque levels, instead of pixels. When calculating the dose, the value for such exposure is correctly calculated. The pixel size is taken to be the pixel pitch, or 2.6µm. From Equation 2.5, this shows that the normalized intensity should be zero and therefore the contribution from the opaque pixel will be zero. However, in practice, gray levels with an opaque pixel for one of the two exposures occur higher than designed. This means the dose is actually lower than calculated. A profile illustrating this effect is shown in Figure 4.13 and an example SEM follows in Figure 4.14.

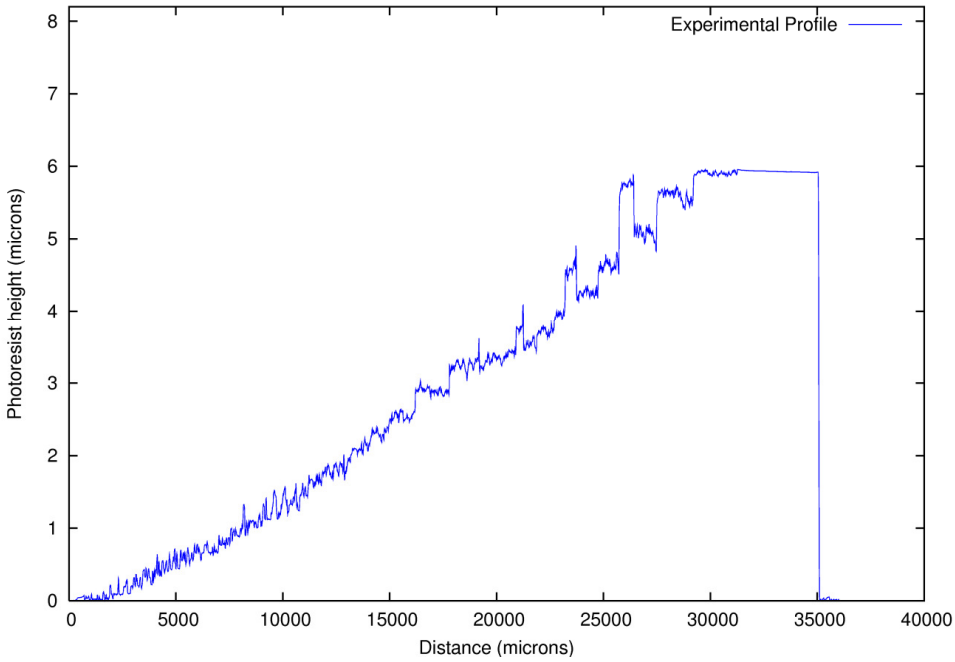

Figure 4.13: Measured stylus profile of a wedge that used "opaque" levels. The three most prominent plateaus in the profile result from opaque gray levels.

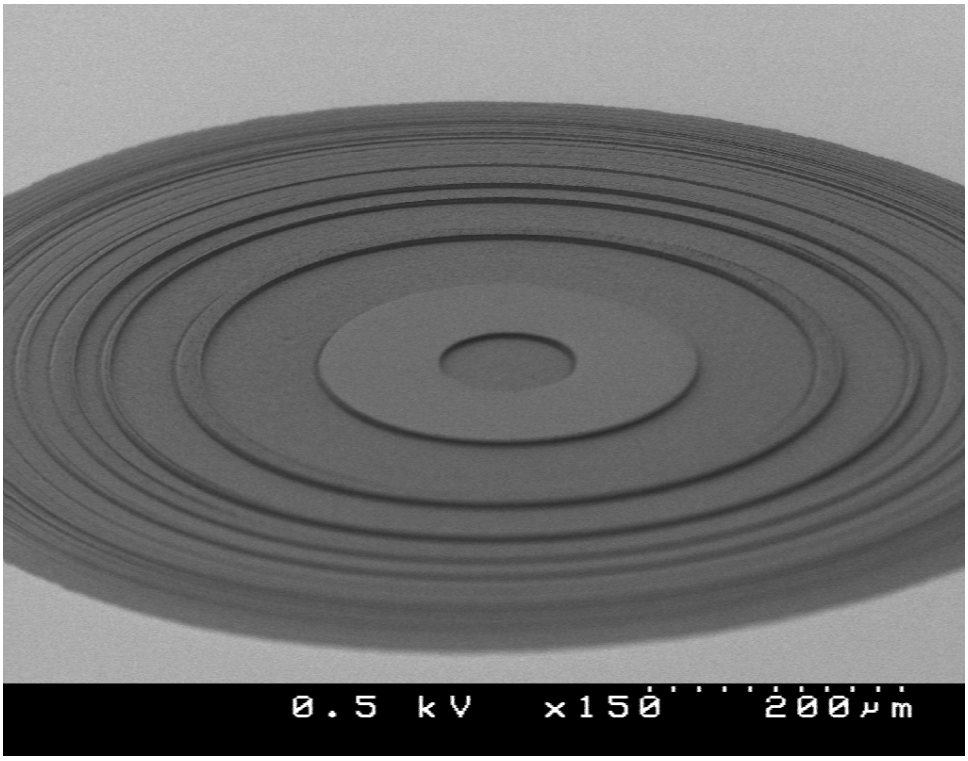

Figure 4.14: SEM of a dome structure. The more elevated levels contain an opaque pixel size during the first exposure.

One likely explanation for this phenomenon comes from a failure in the initial commutability experiments. It is obvious that an exposure will commute with itself if one of the exposures is completely blocked because, in reality, there is only one exposure. From Equations 3.2 and 3.3, the absorption coefficient of the photoresist changes as the photoresist is exposed. Since the exposures were found to be commutable, it was assumed that changes in absorption coefficient had little effect on the exposure depth. This is true, but neglects a very subtle point. The first exposure changes the absorption coefficient to about the same value for all doses used in this thesis, and therefore the photoresist condition is altered to the same

degree. However, the subtlety comes in when using an opaque level for the first exposure. Since no intensity reaches the photoresist, the absorption coefficient does not change. Therefore, the second exposure has a harder time penetrating the photoresist and creates a higher gray level than expected. The calibration is created to "assume" the absorption coefficient has decreased, but when the first exposure is opaque, the resulting dose will be lower than expected. This effect was simulated with the same algorithm used to investigate the commutation effect in Section 3.3. A double-exposure was simulated using a pixel size of 1.0 µm and an exposure time of 0.5 seconds followed by a pixel size of 2.0 µm and an exposure time of 1.0 second (Figure 4.15).

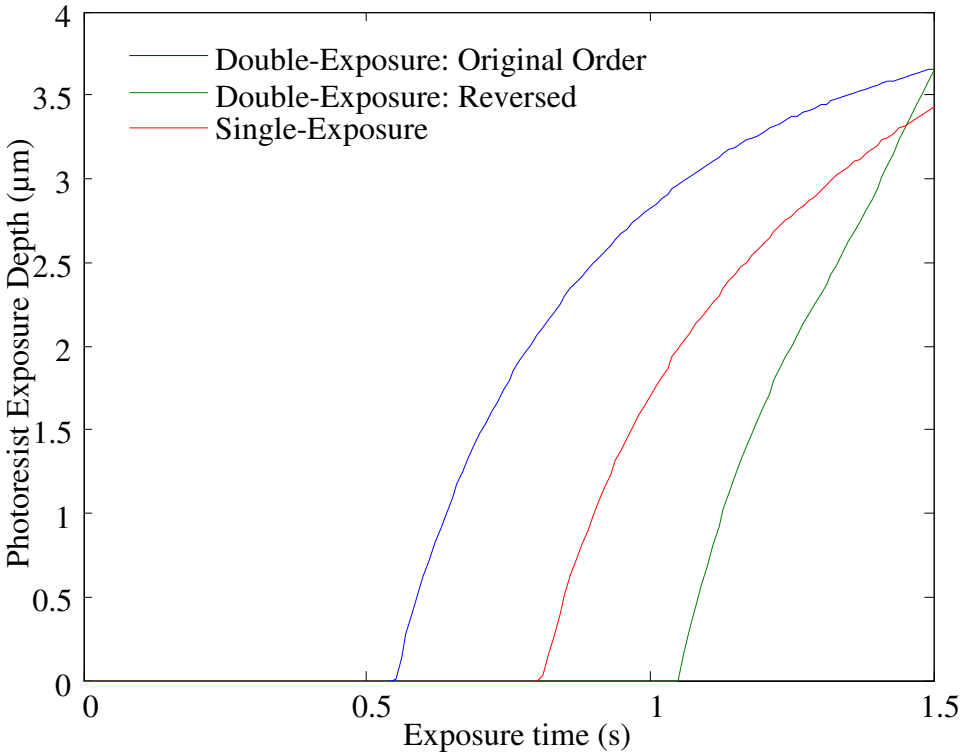

Figure 4.15: Simulation of double-exposure and single-exposure photolithography. All exposures have the same total dose, but the single-exposure (red) does not expose as far into the photoresist.

As before, the exposure order was reversed, but in addition a single-exposure was simulated that had the same total dose. The single-exposure penetrated the photoresist 0.22 μm less than the double-exposures. This analysis adequately explains why the opaque features did not develop as predicted. Since this effect is inherent to the calibration process, the most direct solution is to calibrate the opaque exposures separately from the double-exposure gray-scale regions. If the exposures do not commute, a more complete calibration technique will be required that considers this effect.

Chapter 5

Summary and Future Work

5.1 Summary

This thesis presents the development of a double-exposure gray-scale photolithography fabrication technique to realize 3D structures with a higher vertical resolution compared to single-exposure photolithography. This technology was developed on the foundation of pixelated gray-scale masks, which have a vertical resolution that is limited by the mask fabrication and projection photolithography process. The double-exposure technique was successful in overcoming this limitation by adding a second pixelated mask exposure to achieve greater control over the photoresist profile. It has been demonstrated that this technique successfully improved the existing fabrication technology without increasing the complication of the mask fabrication process and only required one additional photolithography step.

The design of any pixelated gray-scale mask requires a calibration curve, but the calibration approach developed for single-exposure gray-scale photolithography was not sufficient to calibrate double-exposure photolithography.

Therefore, a more sophisticated calibration scheme was developed that included data collection, automated data analysis and curve fitting. The theoretical relationship between the size of pixels on the mask and the resulting photoresist height was examined, but an experimental procedure was selected to empirically determine this relationship. A computer simulation used the resulting calibration curve to better understand the photolithography process and calculate optimal values of the exposure time ratio. After fully calibrating this photolithography technique, a computer-assisted design tool helped create mask layout files to realize double-exposure test structures.

This fabrication technology was utilized to create a variety of wedges, bowls and domes. Not only did the structures fabricated by double-exposure photolithography match the designed profile, they were more accurate to the designed profile than those fabricated by single-exposure photolithography. This result proves the improvement in the vertical resolution. The vertical resolution is quantitatively represented by the average and maximum step height, and the average step height was improved by an order of magnitude, decreasing from 0.19 μm using single-exposure photolithography to 0.02 μm using double-exposure. The maximum step height also showed a two-fold improvement, decreasing from 0.4 μm to 0.2 μm from single-exposure to double-exposure, respectively. These results show that the addition of a second gray-scale exposure is a viable fabrication technology that can be applied for nearly any desired photoresist profile.

The ability to calculate the expected photoresist height when given two exposure times and pixel sizes is very important and powerful. Using this capability, higher-order effects of double-exposure photolithography could be examined. In this thesis, the effect of mask misalignment was simulated to better understand why roughness occurs on some profiles. It was possible to simulate this effect by calculating the dose that would be produced if the masks were shifted slightly relative to each other. Once the modified dose was calculated, the resulting photoresist profile was determined using the calibration curve. This misalignment effect was examined, and it was shown that misalignment could indeed be causing the roughness observed along profiles. The simulation helped identify the probable source of the effect, and allowed the creation of a "design rule" to build in some tolerance for misalignment into the mask design itself. The design rule was applied to a mask design of a similar structure, and the same misalignment simulation was performed. The improved mask design was simulated to show a decreased roughness in the presence of misalignment. This example clearly shows the power of being able to simulate exposure effects using the calibration curve and computer simulations.

5.2 Future Work

This thesis presents the first demonstration of a new double-exposure photolithography technique. This work sets the foundation for future research into

high-resolution 3D photolithography, and will hopefully enable an accelerated study that makes pixelated gray-scale technology available for a wider variety of researchers. While the groundwork is demonstrated, further research is required to fully realize the potential of this new fabrication technology.

5.2.1 Non-Square Pixels

The pixelated masks in this work use a self-restricting limitation of square pixel geometries for design simplicity. In actuality, rectangular pixels may also be utilized to increase the number of pixel sizes available, which will increase the number of gray levels. Even using rectangular pixels, single-exposure photolithography is still limited to about fifty pixel sizes. This limitation still cannot provide a vertical resolution that compares to continuous-tone photolithography. However, if rectangular pixels were applied with double-exposure photolithography, it would be theoretically possible to realize 2500 unique gray levels in photoresist. If it becomes possible to reliably realize this many gray levels, the technology will be able to fabricate effectively continuous profiles.

5.2.2 Lower resolution mask writers

Double-exposure photolithography does not only present the ability to only improve the vertical resolution of existing mask technologies. This technique also presents the ability for mask writing tools to produce gray-scale masks that were

never considered before. For example, cheaper, lower-resolution mask writers can only create a handful of pixel sizes and are therefore not ideal for producing gray-scale masks. However, the double-exposure photolithography technique enables lower-resolution mask writers to realize enough gray levels to be useful. If only seven different rectangular pixel sizes are possible, double-exposure would allow designs with up to 49 gray levels. This is not sufficient to fabricate structures that need high-resolution profiles, but is capable of realizing structures that have lower resolution requirements. In other words, structures that can only be fabricated using more expensive high-resolution chrome masks could then be fabricated using much cheaper mask writing technology.

5.2.3 Including Opaque Levels

As described in section 4.5, opaque gray-levels are defined as a gray level where one of the masks is complete opaque, and the other is a gray-scale pixel. These levels are desired because they allow new dose possibilities, and therefore increase the number of gray levels. However, due to differences in exposure kinetics for single-exposure and double-exposure photolithography, these opaque exposures are not compatible with the existing calibration method. The most immediate solution, which was applied in this thesis, was to simply not use these levels. If the calibration method is modified to handle opaque exposures separately, it may be possible to create designs that use a wider range of UV intensities. Since

the largest steps between gray levels occurs at the lower end of the UV transmission range, this would help further increase the vertical resolution by decreasing the maximum step size.

5.2.4 New modeling techniques

The modeling and simulations scheme presented here allows investigation of critical fabrication tolerances, such as mask alignment. Following this example, other higher-order effects can be examined to further improve the technology. For example, the effect of the width of each gray level could be examined. At the moment, there is no design rule that limits how many pixels are required to define a single gray level, and some designs have gray levels with only a few pixels. This is likely to cause a blending effect with neighboring pixels due to diffraction, and may result in undesired exposure combinations, similar to the issue with mask misalignment. By investigating this effect, it may be possible to develop another design rule that protects structures from this issue. If this and other effects are explored, resulting design rules can be combined into a comprehensive design tool for intelligent double-exposure gray-scale mask creation towards fabrication of complex 3D silicon devices.

Appendix I: Source Code

A1 Empirical Data Processing

```
1; #Function file
#This file contains functions to processes data from exposures
using either the DEGS1 or DEGSB (DEGS-old) masks.
#Define option defaults:
ploteach = 0;
plotwhole = 0;
#degsexport is the main driving program which reads a folder
containing scanned files and writes the data in a .csv for further
analysis.
function [depth, dose] = degsexport(folder, type, intensity,
ploteach, plotall)
#DEGS Data extraction function. Writes data from degsread into csv
file "dataf"
#degsexport(foder, type

      #Set pixel sizes by type
      if (type == 1);
          pix =
[2.6,2,1.9,1.8,1.7,1.6,1.5,1.4,1.3,1.2,1.1,1.0,.9,.8,.7,.6,0];
            npix = numel(pix);
      endif
      if (type == 2);
          pix = [2.6,1.8,1.6,1.4,1.2,1.0,.8,.6];
            npix = numel(pix);
      endif

      #Collect data from files
      data = degsread(folder, pix, ploteach, plotall);
      #Extract file information
      file = readdir(folder){3};
      row=file(findstr(file,"r")+1:findstr(file,"r")+3); #Row exp
in sec
      column=file(findstr(file,"c")+1:findstr(file,"c")+3);#Column
exp
      die=file(findstr(file,"d")+1:findstr(file,"d")+2);   #Die
number
      wafer=file(findstr(file,"w")+1:findstr(file,"w")+2); #Waf
number

      #Convert data array to 1-D
      k=1;
      for (r = 2:numel(data(1,:)))
            for (c = 2:numel(data(:,1)))
                  height(k) = data(r,c);
                  pr(k) = data(r,1);      #Row pix size (scan
direction)
```

```
                pc(k) = data(1,c);      #Pixel size on the column
                k++;
            end
        end
        pitch = max(pc);
        prheight = max(data(:,2));
        #tr = (pitch^2 - pr.^2)/pitch^2; old way of calculating pitch
        #tc = (pitch^2 - pc.^2)/pitch^2; old way of calculating pitch

        #Pixel size scaling to compensate for mask error
        pr=pr+0.05;
        pc=pc+0.05;
        tr = (1 - pr.^2./pitch^2).^1;
        tc = (1 - pc.^2./pitch^2).^1;
        dose = intensity * (tr*str2num(row)+tc*str2num(column));
        idx = find(height > 0);
        dose = dose(idx);
        height = height(idx);
        depth = prheight - height;
        #depth = height;
        #outdata(:,1) = dose;

        #Write data
        fname = sprintf("%sdata_r%s_c%s_d%s_w%s.csv",
"/home/lmosher/Profiles/", row, column, die, wafer);
        csvwrite(fname, data);
        fname = sprintf("%sdose_r%s_c%s_d%s_w%s.csv",
"/home/lmosher/Profiles/", row, column, die, wafer);
        csvwrite(fname, [dose', depth']);
end
```

#Reads a folder and returns a data array containing the pixels, exposure times and the corresponding gray level height

```
function data = degsread(folder, pix, ploteach, plotall)
#DEGS Processing function - Extracts heights from a DEGS grid
profile
#degsp(folder, type)
#folder = Data folder w/ files of form:
mMASK_pPIXEL_rEXP1_cEXP2_dDIE_wWAF
#           _rEXP1 is exp time of row, _rEXP2 is the column
#type = The profile type:
#     1 = DEGS1 mask, 2.6 grid
#     2 = DEGS-brian mask, 2.6 grid
#     3 = DEGS1 mask, 2.8 grid
#Default options
        slope = 0.1;            #Target slope of y in um/um
        w = 0.05;               #Width of RCF in um

        #Build data array
        npix = numel(pix);
        data(2:npix+1) = pix;
        data(2:npix+1,1) = pix';
        datax(2:npix+1) = pix;
```

```
      datax(2:npix+1,1) = pix';

      #Build file list
      files = readdir(folder);

      #Go through each file and extract data
      for (k = 1:numel(files)-2)
            k;
            file = files{k+2};

            #Read input file, convert y from Ang to um
            scan=csvread(sprintf("%s%s",folder,file));
            x=scan(39:numel(scan(:,2)),1);
            y=scan(39:numel(scan(:,2)),2)/10000;
            dx= mean(diff(x));      #Derivative of x

            #Read file information
            p=file(findstr(file,"p")+1:findstr(file,"p")+3); #Pix
size
            dataidx=find(data(2:18,1) == str2num(p))+1;

            #Determine direction of wedge, convert to decreasing
            if ( mean(y(1:floor(numel(y)/2))) <=
mean(y(floor(numel(y)/2):numel(y))))
                  y = y(-(1:numel(y))+numel(y)+1);
            endif

            #Separate each box and perform Random Consensus Filter
            done=0;
            i = 1;

            while (done != 1)
                  #Clear variables
                  num=[];idx=[];le=[];te=[];
                  #Find leading edge (min element w/(adjusted)
slope)
                  s = diff(y)/dx;
                  adjslope = 1.5.^-i*0.15 + 0.02;
#Above was Experimentally determined. Ranges from 0.1 to 0.02
                  le = min(find(s >= adjslope));
                  if (length(le) == 0)
                        done = 1;
                        continue
                  endif

                  #Find the end of this box (max of x < le + 150um)
                  boxend = max(find(x <= x(le)+150))-1;

                  #Find trailing edge
                  te = (le:boxend)(max(find(s(le:boxend) <= -
adjslope)));
                  if (length(te) == 0)
                        done = 1;
```

```
                        continue
                  endif

                  #Redefine regions, delete until boxend for next
loop
                  thisx = x(le:te);
                  thisy = y(le:te);
                  x = x(boxend:numel(x));
                  y = y(boxend:numel(y));
                  #Perform Random Consensus Filter selection
                  w = max(thisy)/50;
                  window = linspace(min(thisy), max(thisy),
max(thisy)/(w/10));
                  for (j=1:numel(window));
                        num(j) = sum((thisy >= window(j)-w/2) &
(thisy <= window(j) + w/2));
                  endfor
                  idx = round(median(find(num == max(num))));
                  data(dataidx,i+1) = mean(thisy(find( (thisy >=
window(idx) - w/2) & (thisy <= window(idx) + w/2))));
                  datax(dataidx,i+1) = mean(thisx(find( (thisy >=
window(idx) - w/2) & (thisy <= window(idx) + w/2))));
                  i++;
                  #Data sanity checks
                  if (i >= 18)
                        done = 1;
                  endif
                  #Stop collecting data under 0.095um
                  if (data(dataidx,i) <= 0.095)
                        done = 1;
                  endif
                  #Override data below 0.07um (don't trust)
                  if (data(dataidx,i) <= 0.07)
                        data(dataidx,i) = 0;
                  endif
                  #Plot each step w/ selected point
                  if (ploteach == 1)
                        plot(thisx,thisy,
thisx,data(dataidx,i)*ones(1,numel(thisx))-w/2,"3",
thisx,data(dataidx,i)*ones(1,numel(thisx))+w/2,"3")
                        #sleep(1)
                  endif
            end
            if (plotall == 1)
                  x=scan(39:numel(scan(:,2)),1);
                  y=scan(39:numel(scan(:,2)),2)/10000;
                  if ( mean(y(1:floor(numel(y)/2))) <=
mean(y(floor(numel(y)/2):numel(y))))
                        y = y(-(1:numel(y))+numel(y)+1);
                  endif
                  plot(x, y,
datax(dataidx,2:numel(data(dataidx,:))),
data(dataidx,2:numel(data(dataidx,:))), "35")
```

```
                  sleep(2)
            endif
      end
end
```

#This function calculates the ideal exposure ratio given a calibration curve and the total exposure time.

```
function ul = ratio()

ratio = 1;
total = 2.6;
delta = 0.1;
sign = 1;
dose = 0; x = 0; idx = 0; m = 0;
exp2 = total/(1+ratio);
exp1 = total - exp2;

dose = ((pitch^2 - pixel1.^2) ./ pitch^2) .* exp1 + ((pitch^2 -
pixel2.^2) ./ pitch^2) .* exp2;

depthnew = -8.85 + 15.11.* (1 - exp( -3.30 * dose));
mold = max(diff(depthnew));

for i = 1:1000

      ratio = ratio + delta*sign;

      exp2 = total/(1+ratio);
      exp1 = total - exp2;

      dose = ((pitch^2 - pixel1.^2) ./ pitch^2) .* exp1 + ((pitch^2
- pixel2.^2) ./ pitch^2) .* exp2;

      x = 0:total:max(x1);
      idx = find(dose < max(dose));
      dose = dose(idx);
      x = x(idx);

      depthnew = -8.85 + 15.11.* (1 - exp( -3.30 * dose));
      m = max(diff(depthnew));
      if (m < mold)
            delta = delta*0.95;
      endif
      if (m > mold)
            delta = delta*1.05;
            sign = sign*-1;
      endif
      mold = m;
end
ul = ratio;
end
```

A2 Mask Design Program

```
1; #Defines file as a function file
#Double Exposure Gray Scale Modeling
#heightlist(pitch, model, exp1, exp2, fablimits)

#Build_structure is the driving program to define a structure:
function [x, y, p1, p2, z, h] = build_structure(fname, structure,
model, pitch, prthick, exp1, exp2, dim1, dim2, dim3, fablimits)
   if (nargin < 11)
      if (nargin == 10)
      fablimits = [1, 0.2];
      else
        printf "Usage: build_structure(fname, structure, model,
pitch, prthick, exp1, exp2, dim1, dim2, dim3, fablimits)\n"
      return
      endif
   endif
   [h, p1, p2] = heightlist(pitch, model, prthick, exp1, exp2,
fablimits);
   [x, y, p1, p2, z] = pixmap(h, p1, p2, pitch, structure, dim1,
dim2, dim3);
   write_structure(fname, x, y, p1, p2, structure);
endfunction

#Write_structure writes the mask layout files for the structure
function write_structure(fname, x, y, p1, p2, structure)
   if (numel(x) != numel(y)) y(1:numel(x)) = y; endif
   mask1fid = fopen(["/home/lmosher/", fname, "1.tco"], "at");
   mask2fid = fopen(["/home/lmosher/", fname, "2.tco"], "at");
   for i=1:numel(x)
      if (p1(i) != 0)
       fprintf(mask1fid, "box %1.1f %1.1f !%1.1f !%1.1f\n", p1(i),
p1(i), x(i), y(i));
      endif
      if (p2(i) != 0)
         fprintf(mask2fid, "box %1.1f %1.1f !%1.1f !%1.1f\n",
p2(i), p2(i), x(i), y(i));
      endif
   endfor
   fclose(mask1fid);
   fclose(mask2fid);
endfunction


#Heightlist provides the gray level heights.
function [height, pixel1, pixel2, h2] = heightlist(pitch, model,
prthick, exp1, exp2, fablimits)

#Generates heightlist, which is an array of heights and the two
pixels to produce each height
#Inputs:
```

```
#pitch -       The pitch for the gray scale levels
#model -       The model number:
#  1: Logaritmic: Single curve depth vs. dose fit w/ Brian's data
#  2: Exponential rise to max
#prthick -     Photoresist thickness in microns
#exp1/exp2 -   Exposure times in seconds
#fablimits -   Fabrication limits in [minfeaturedistance,
minspotsize] in microns
#     Minfeaturedistance is the smallest distance between pixels.
Defaults 0.5 microns
#     Minspotsize is the incrimental size of a pixel. Defaults 0.1
microns
   if (nargin < 6)
      if (nargin == 5)
      fablimits = [1, 0.2];
      else
        printf "Usage: heightlist(pitch, model, prthick, exp1,
exp2, fablimits)\n"
      return
      endif
   endif

#Built array of possible pixels
   if (numel(fablimits) < 3)
      pixels(1) = 0;
      j = 2;
      for i = fablimits(1):fablimits(2):pitch-fablimits(1)
       pixels(j) = i;
       j++;
      endfor
      pixels(j) = pitch;
   else
      pixels = fablimits;
   endif

#Loops through pixels. First loop is exposed to exp1, second to
exp2. Calculate height based on mode.

   pp = pixels'*ones(1,numel(pixels));
   pixel1 = pp'(1:numel(pp));
   pixel2 = pp(1:numel(pp));
   dose = ((pitch^2 - pixel1.^2) ./ pitch^2) .* exp1 + ((pitch^2 -
pixel2.^2) ./ pitch^2) .* exp2;
      if (exp2 == 0)
       #dose = ((pitchdd^2 - pixels.^2) ./ pitch^2) .* exp1;
          pixel1 = pixels;
          pixel2 = pixels;
          exp1 = exp1/2;
          exp2 = exp1;
          dose = ((pitch^2 - pixel1.^2) ./ pitch^2) .* exp1 +
((pitch^2 - pixel2.^2) ./ pitch^2) .* exp2;
      endif
   if (model == 1)
```

```
      idx = find(dose > 0);
      dose = dose(idx);
      pixel1 = pixel1(idx);
      pixel2 = pixel2(idx);
      depth = 4.8889 + 2.8089 .* log(dose - 0.0827);
   elseif (model == 2)
      depth = -8.85 + 15.11 .* (1 - exp( -3.30 * dose));
      depth(find(depth < 0)) = 0;
   endif

   height = prthick - depth;
   idx = find(height >= 0);
   height = height(idx);
   pixel1 = pixel1(idx);
   pixel2 = pixel2(idx);
endfunction

#Pixmap builds (x,y,z) coordinates for a desired structure
function [x, y, pixel1, pixel2, z] = pixmap(height, pixel1, pixel2,
pitch, structure, dim1, dim2, dim3)
#height - heights from heightlist
#pixel1/2 - pixels from heightlist
#structure type:
# 1: ramp
# 2: bowl
# 3: Turbine
# 4: Race
# 5: Dome
#dim1/2/3 - Dimensions for structure
# 1/2/3: Ramp height, length, unused, respectively
# Bowl: 1 = height, 2 = radius, 3 = unused
   [height, sortidx] = sort(height);
   pixel1 = pixel1(sortidx);
   pixel2 = pixel2(sortidx);
   if (structure == 1)
      #Build ramp by finding closest available height under dim1
(height)
      hmax = max(find(height <= dim1));
      height = height(1:hmax);
      pixel1 = pixel1(1:hmax);
      pixel2 = pixel2(1:hmax);
      sortidx = sortidx(1:hmax);
      #Find the equation for the buildable ramp
      b = 0;
      m = height(hmax)/dim2;
      #Build array of x values spaced by the pitch
      x = 0:pitch:dim2;
      x(numel(x) + 1) = max(x) + pitch;
      #Cycle down the height value index, starting with the max
      y = x*m + b;
      for i = 1:hmax
       xidx(i) = min(find(y >= height(i)));
      endfor
```

```
      midpts(1) = 1;
      midpts(2:numel(xidx)) = round(diff(xidx)/2 +
xidx(1:numel(xidx)-1));
      midpts(numel(midpts)+1) = xidx(numel(xidx));
      j = 1;
      for i = 1:numel(midpts)-1
       y(midpts(i):midpts(i+1)) = height(j);
       p1(midpts(i):midpts(i+1)) = pixel1(j);
       p2(midpts(i):midpts(i+1)) = pixel2(j);
       j++;
       endfor
       pixel1 = p1;
       pixel2 = p2;
       z = y;
       y(1:numel(y)) = 0;
   endif
   if (structure == 2)
      hmax = max(find(height <= dim1));
      height = height(1:hmax);
      pixel1 = pixel1(1:hmax);
      pixel2 = pixel2(1:hmax);

      #Perform some crazy algebra to avoid nested for loops
      x = 0:pitch:dim2;
      xx = x'*ones(1,numel(x));
      x = xx(1:numel(xx));
      y = xx'(1:numel(xx));

      #Eliminate points with angle over 45 degrees
      idx = find(atan(y./x) <= pi()/4);
      idx = [1,idx];
      x = x(idx);
      y = y(idx);

      #Calculate radius and find points within device radius
      r = sqrt(x.^2 + y.^2);
      idx = find(r <= dim2);
      r = r(idx);
      x = x(idx);
      y = y(idx);

      #Define height as an inverse oblate spheroid: h = dim1*(1-
sqrt(1-r^2/R^2));
      h = dim1*(1-sqrt(1-r.^2/(dim2^2)));
      for i = 1:numel(height)
       if (i == 1)
          idx = find (h <= height(1));
          z(idx) = height(1);
          p1(idx) = pixel1(1);
          p2(idx) = pixel2(1);
       endif
       idx = find(h >= height(i));
       z(idx) = height(i);
```

```
        p1(idx) = pixel1(i);
        p2(idx) = pixel2(i);
      endfor
      pixel1 = p1;
      pixel2 = p2;
   endif
   if (structure == 3)
      hmax = max(find(height <= dim1));
      height = height(1:hmax);
      pixel1 = pixel1(1:hmax);
      pixel2 = pixel2(1:hmax);

      #Perform some crazy algebra to avoid nested for loops
      x = 0:pitch*2:dim2;
      xx = x'*ones(1,numel(x));
      x = xx(1:numel(xx));
      y = xx'(1:numel(xx));
      xx = 0;

      #Eliminate points with angle over 45 degrees
      idx = find(atan(y./x) <= pi()/4);
      idx = [1,idx];
      x = x(idx);
      y = y(idx);
      idx = 0;

      #Calculate radius and find points within device radius
      r = sqrt(x.^2 + y.^2);
      idx = find(r <= dim2);
      r = r(idx);
      x = x(idx);
      y = y(idx);
      idx = 0;

      #Remove points before compressor surface
      idx = find(r >= dim3);
      r = r(idx);
      x = x(idx);
      y = y(idx);
      idx = 0;

      #Define height as linear function: h = slope*(radius -
offset)
      h = dim1/dim3*(r - (dim2 - dim3));
      for i = 1:numel(height)
       if (i == 1)
          idx = find (h <= height(1));
          z(idx) = height(1);
          p1(idx) = pixel1(1);
          p2(idx) = pixel2(1);
       endif
       idx = find(h >= height(i));
       z(idx) = height(i);
```

```
    p1(idx) = pixel1(i);
    p2(idx) = pixel2(i);
   endfor
   pixel1 = p1;
   pixel2 = p2;
endif
if (structure == 4)
   hmax = max(find(height <= dim1));
   height = height(1:hmax);
   pixel1 = pixel1(1:hmax);
   pixel2 = pixel2(1:hmax);

   #Perform some crazy algebra to avoid nested for loops
   x = 0:pitch*2:dim2;
   xx = x'*ones(1,numel(x));
   x = xx(1:numel(xx));
   y = xx'(1:numel(xx));
   xx = 0;

   #Eliminate points with angle over 45 degrees
   idx = find(atan(y./x) <= pi()/4);
   idx = [1,idx];
   x = x(idx);
   y = y(idx);
   idx = 0;

   #Calculate radius and find points within device radius
   r = sqrt(x.^2 + y.^2);
   idx = find(r <= dim2-2875);
   r = r(idx);
   x = x(idx);
   y = y(idx);
   idx = 0;

   #Remove points before race surface
   idx = find(r >= dim3+2875);
   r = r(idx);
   x = x(idx);
   y = y(idx);
   idx = 0;

   #Define height for inner radius and outer radius
   #idx = find( (r <= dim3+2875) | (r >= dim2-2875) );
   #z(idx) = height(hmax);
   #p1(idx) = pixel1(hmax);
   #p2(idx) = pixel2(hmax);
   #idx = 0;

   #Define bottom bowl area
   idx = find( (r <= dim2-2875-700) & (r >= dim3+2875+700) );
   z(idx) = min(height);
   p1(idx) = min(pixel1);
   p2(idx) = min(pixel2);
```

```
      idx = 0;

      #Define height down first slope with h = -slope*(radius -
offset) + hmax. x dim = 700u which is 140u on wafer
      idx = find( (r <= dim3+2875+700) & (r >= dim3+2875));
      h =  dim1 - dim1/700*(r(idx) - (dim3+2875));
      for i = 1:numel(height)
       if (i == 1)
          id2 = find (h <= height(1));
          z(idx(id2)) = height(1);
          p1(idx(id2)) = pixel1(1);
          p2(idx(id2)) = pixel2(1);
       endif
       id2 = find(h >= height(i));
       z(idx(id2)) = height(i);
       p1(idx(id2)) = pixel1(i);
       p2(idx(id2)) = pixel2(i);
      endfor

      #Define height up second slope with h = slope*(radius -
offset). x dim = 700u which is 140u on wafer
      idx = find( (r <= dim2-2875) & (r >= dim2-2875-700));
      h =  dim1 + dim1/700*(r(idx) - (dim2-2875));
      for i = 1:numel(height)
       if (i == 1)
          id2 = find (h <= height(1));
          z(idx(id2)) = height(1);
          p1(idx(id2)) = pixel1(1);
          p2(idx(id2)) = pixel2(1);
       endif
       id2 = find(h >= height(i));
       z(idx(id2)) = height(i);
       p1(idx(id2)) = pixel1(i);
       p2(idx(id2)) = pixel2(i);
      endfor

      pixel1 = p1;
      pixel2 = p2;
   endif
   if (structure == 5)
      hmax = max(find(height <= dim1));
      height = height(1:hmax);
      pixel1 = pixel1(1:hmax);
      pixel2 = pixel2(1:hmax);

      #Perform some crazy algebra to avoid nested for loops
      x = 0:pitch:dim2;
      xx = x'*ones(1,numel(x));
      x = xx(1:numel(xx));
      y = xx'(1:numel(xx));

      #Eliminate points with angle over 45 degrees
      idx = find(atan(y./x) <= pi()/4);
```

```
      idx = [1,idx];
      x = x(idx);
      y = y(idx);

      #Calculate radius and find points within device radius
      r = sqrt(x.^2 + y.^2);
      idx = find(r <= dim2);
      r = r(idx);
      x = x(idx);
      y = y(idx);

      #Define height as an inverse oblate spheroid: h =
dim1*(sqrt(1-r^2/R^2));
      h = dim1*(sqrt(1-r.^2/(dim2^2)));
      for i = 1:numel(height)
       if (i == 1)
          idx = find (h <= height(1));
          z(idx) = height(1);
          p1(idx) = pixel1(1);
          p2(idx) = pixel2(1);
       endif
       idx = find(h >= height(i));
       z(idx) = height(i);
       p1(idx) = pixel1(i);
       p2(idx) = pixel2(i);
      endfor
      pixel1 = p1;
      pixel2 = p2;
   endif
endfunction
```

A3 Data Analysis Program

```
1; #Function File
#DEGS Analysis Functions

#mwedge calculates the "modeled wedge" (or other structure) by
reading #in the pixel design for each mask and using the pixel
calibration to #predict the photoresist profile

#This function can also predict mask misalignments if the "align"
variable is defined
function [mx, md, mh, mhu, mhl, mdose] = mwedge(exp1, exp2, o, s,
ave, align)
#Calculate the Model Wedge
#This function takes the developometer pixels and calculates the
modeled wedge based on modeled datapoints
#The "developometer" was a particularly large wedge used for visual
indication of development

      #Read in mask pixels
      dat = csvread("/home/lmosher/gswedge.csv");
#     dat = csvread("/home/lmosher/gsbowl.csv");
#     dat = csvread("/home/lmosher/gsbowl1.csv");
#     dat = csvread("/home/lmosher/gsbowl7.csv");
      x = dat(:,1);
      x = x/5;
      pixel1 = dat(:,2);
      pixel2 = dat(:,3);

      #Calculate dose

      pixel1 = (pixel1+o)*s;
      pixel2 = (pixel2+o)*s;
      #o and s offset and scale the pixel size to compensate for
mask error (usually used as 0 and 1, but included for
experimentation)


      pitch=2.6;
      dose = ((pitch^2 - pixel1.^2) ./ pitch^2) .* exp1 + ((pitch^2
- pixel2.^2) ./ pitch^2) .* exp2;
      doseu = ((pitch^2 - ((pixel1+o)*s).^2) ./ pitch^2) .* exp1 +
((pitch^2 - ((pixel2+o)*s).^2) ./ pitch^2) .* exp2;
      dosel = ((pitch^2 - ((pixel1-o)*s).^2) ./ pitch^2) .* exp1 +
((pitch^2 - ((pixel2-o)*s).^2) ./ pitch^2) .* exp2;

      idx1 = find(pixel1 == 2.6);
      idx2 = find(pixel2 == 2.6);

      #If alignment is defined, interpolate pixels and re-define
dose
      if (align != 0)
```

```
            intpx = 0:0.05:max(x);
#           intpx = x;
            for i=1:numel(intpx) idx(i) = max(find(x <= intpx(i)));
end   #Interpolate pixels
            idx(find(idx==0)) = 1;
                        #Set 0 idxs to 1
            d1 = ((pitch^2 - pixel1(idx).^2) ./ pitch^2) .* exp1;
            d2 = ((pitch^2 - pixel2(idx).^2) ./ pitch^2) .* exp2;

            if (align > 0)
                  d2 = [d2'(align:numel(d2)), zeros(1,align-1)]';
            end
            if (align < 0)
                  align = abs(align);
                  d1 = [d1'(align:numel(d1)), zeros(1,align-1)]';
            end

            x = intpx;

            if (ave != 0)
                  for i=1:ave:numel(x)-ave
                        d1a((i+ave-1)/ave) = mean(d1(i:i+ave));
                        d2a((i+ave-1)/ave) = mean(d2(i:i+ave));
                        xa((i+ave-1)/ave) = mean(x(i:i+ave));
                  end
                  d1 = d1a;
                  d2 = d2a;
                  x = xa;
            end
            dose = d1+d2;
      end


      #Cut off max dose (eliminates vertical line)
      idx = find(dose < max(dose));
      mdose = dose(idx);
#     mdoseu = doseu(idx);
#     mdosel = dosel(idx);
      mx = x(idx);

      #Fit parameters (paste these in from QtiPlot)
y0  = -8.85397275177411;
A  = 15.1093746319895;
t  = 3.30177704736193;


      #Pixels unsized
#     y0  = -8.43339770739965;
#     A  = 14.4407449080681;
#     t  = 2.11071712626456;

      #Pixels sized + 0.05
#     y0  = -6.82240040795222;
```

```
#     A  = 12.7780184166085;
#     t  = 2.03894307144594;

      md=y0+A*(1-exp(-mdose*t));
#     mdu=y0+A*(1-exp(-mdoseu*t));
#     mdl=y0+A*(1-exp(-mdosel*t));
      mh=max(md) - md;
#     mhu=max(mdu) - mdu;
#     mhl=max(mdl) - mdl;
end
```

#This function reads in the "experimental wedge" for comparison to the modeled wedge created from above.

```
function [ex, ed, eh] = ewedge(file);
#Read in the experimental wedge profile

      scan = csvread(file);
      ex=scan(39:numel(scan(:,2)),1);
      eh=scan(39:numel(scan(:,2)),2)/10000;
      ed = max(eh) - eh;
end



function plotcurves(ex, ey, mx, my, dy);
```

#Facilitate simple plotting of above data

```
      plot(mx./5, my+dy, "1;Model;", ex, ey, "3;Experimental;");
end
```

#edose finds the "experimental dose" that most closely matches the modeled dose. It simply allows plotting both the modeled wedge and the experimental wedge using the same dose values.

```
function edose = edosefind(ex, mx, mdose)
#Find edose by finding nearest mx to each ex and using (mx, mdose)
      for i=1:numel(ex)
            midx = max(find(mx < ex(i)));
            edose(i) = mdose(midx);
      end
end

function y = linfunc(x)
      if (x <= 100) y = 0; end
      if (x >= 100) y = 0.002*(x-100); end
      if (x >= 200) y = 0.0025*(x-200) + 0.2; end
      if (x >= 400) y = 0.00325*(x-400) + 0.7; end
      if (x >= 600) y = 0.00375*(x-600) + 1.35; end
      if (x >= 800) y = 0.0025*(x-80) + 2.1; end

end
```

Bibliography

[1] C. Linder, L. Paratte, M-A Gretillat, V.P. Jaeckllin, and N.F. de Rooij, "Surface Micromachining," J. *Micromech. Microeng.*, vol. 2, pp. 122-132, 1992.

[2] G. T. A. Kovacs, N. I. Maluf, and K. E. Peterson, "Bulk Micromachining of Silicon," *Proc. IEEE*, vol. 86, pp. 1536-1551.

[3] O.P. Lehar, J.P. Sagan, L. Zhang, and R.R. Dammel, "Solvent Content of Thick Photoresist Films," *Proc. of the SPIE: Advances in Resist Technology and Processing XVII*, vol. 3, pp. 442-451, 2000.

[4] J. M. Bustillo, R. T. Howe, and R. S. Muller, "Surface Micromachining for Microelectromechanical Systems," *Proc. IEEE*, vol. 86, no. 8, pp. 1552-1574, 1998.

[5] D.M. Manos, D.L. Flamm, "Plasma Etching: An Introduction," Academic Press INC., San Diegeo, 1989.

[6] I. W. Rangelow. "Dry Etching-Based Silicon Micro-Machining for MEMS," *Vacuum*, vol. 69, pp. 279-291, 2001.

[7] R. Bosch Gmbh, Patents 4,855,017 and 4,784,720 (USA) and 4241045C1 (Germany).

[8] A.A. Ayón, R. Braff, C.C. Lin, H.H. Sawin, and M.A. Schmidt, "Characterization of a Time Multiplexed Inductively Coupled Plasma Etcher," *J. of the Electrochemical Society*, vol. 146, no. 1, pp. 339-349, 1999.

[9] S.A. McAuley, H. Ashraf, L. Atabo, A. Chambers, S. Hall, J. Hopkins, and G. Nicholls, "Silicon Micromachining Using a High-Density Plasma Source," *J. Phys. D: Applied Physics*, vol. 34, pp. 2769-2774, 2001.

[10] P. Ehbets, H.P. Herzig, D. Prongue, M.T. Gale, "High-efficiency continuous surface-relief gratings for two-dimensional array generation," *Opt. Lett.* Vol. 17, no. 13, pp. 908-910, 1992.

[11] E. Di Fabrizio, F. Romanato, M. Gentili, S. Cabrini, B. Kaulich, J. Susini, R. Barrett, "High-efficiency multilevel zone plates for keV X-rays", *Nature*, vol. 401, pp. 895-898, 1999.

[12] B. Morgan, C. Waits, J. Krizmanic and R. Ghodssi, "Development of a Deep Silicon Phase Fresnel lens using Gray-scale Technology and Deep Reactive Ion Etching," *J. of Microelectromech. Sys. (JMEMS)*, vol. 13, pp. 113-120, 2004.

[13] P. Yao, G. J. Schneider, and D. Prather, "Three-dimensional lithography fabrication of microchannels," *J. Microelectromech. Syst*., vol. 14, no. 4, pp. 799-805, Aug. 2005.

[14] Michael J. Vasile, Raja Nassar, Jushan Xie, "Focused ion beam technology applied to microstructure fabrication", *J. Vac. Sci. Technol. B*, vol. 16, pp. 2499-2505, 1998.

[15] P. Yao, G. J. Schneider, D. Prather, E. Wetzel, and D. O'Brein, "Fabrication of three-dimensional photonic crystals with multilayer photolithography," *Opt. Express*, vol. 13, no. 7, pp. 2370-2376, Apr. 2005.

[16] B. Wagner, H. J. Quenzer, W. Henke, W. Hoppe, W. Pilz, "Microfabrication of complex surface topographies using grey-tone lithography," *Sens. and Actuators A, Phys*., vol. 46, no. 1-3, pp. 89–94, Jan.-Feb. 1995.

[17] C. Waits, B. Morgan, M. Kastantin, R. Ghodssi, "Microfabrication of 3D silicon MEMS structures using gray-scale lithography and deep reactive ion etching", *Sensors and Actuators A (Physical)*, vol. 119, pp. 245-25, 2005.

[18] J. Chung and W. Hsu, "Enhancement on forming complex three dimensional microstructures by a double-side multiple partial exposure method," *J. Vac. Sci. Technol. B*, vol. 25, no. 5, pp. 1671-1678, Sept.-Oct. 2007.

[19] M. Tormen, L. Businaro, M. Altissimo, F. Romanato, S. Cabrini, F. Perennes, R. Proietti, H.-B. Sun, S. Kawata, and E. D. Fabrizio, "3D patterning by means of nanoimprinting, X-ray and two-photon lithography," *Microelectron. Eng.*, vol. 73–74, pp. 535–541, June 2004.

[20] J. Kim, D. C. Joy, S.-Y. Lee, "Controlling resist thickness and etch depth for fabrication of 3D structures in electron-beam grayscale lithography," *Microelectron. Eng*., vol. 84, no. 12, pp. 2859-2864, Dec. 2007.

[21] L. Vivien, X. L. Roux, S. Laval, E. Cassan, and D. Marris-Morini, "Design, realization and characterization of 3-D taper for fiber/micro-waveguide coupling," *IEEE J. Sel. Top. Quantum Electron.*, vol. 12, no. 6, pp. 1354-1358, Nov.-Dec. 2006.

[22] F. Hu and S.-Y. Lee, “Dose control for fabrication of grayscale structures using a single step electron-beam lithographic process,” *J. Vac. Sci. Technol. B*, vol. 21, no. 6, pp. 2672-2679, Nov.-Dec. 2003.

[23] K. Totsu, K. Fujishiro, S. Tanaka, and M. Esashi, “Fabrication of three-dimensional microstructure using maskless gray-scale lithography,” *Sens. Actuators A, Phys*., vol. 130-131, pp. 387–392, Aug. 2006.

[24] A. Bertsch, P. Bernhard, and P. Renaud, “Microsterolithography: concepts and applications,” in P*roc. IEEE Int. Conf. on Emerg. Technol. Factory Autom.*, 2001, pp. 289-298.

[25] W. H. Teh, U. Dürig, G. Salis, R. Harbers, U. Drechsler, R. F. Mahrt, C. G. Smith, and H.-J. Güntherodt, “SU-8 for real three-dimensional subdiffraction-limit two-photon microfabrication,” *Appl. Phys. Lett*., vol. 84, no. 20, pp 4095-4097, May 2004.

[26] A. Bertsch, H. Lorenz, and P. Renaud, “Combining Microstereolithography and Thick Resist UV Lithography for 3D Microfabrication,” *Proc. of IEEE: MEMS ’98*, pp. 18-23, Heidelberg, Germany, 1998.

[27] Y. Opplinger, P. Sixt, J.M. Stauffer, J.M. Mayor, P. Regnault, and G. Voirin, “One-step 3D shaping using a gray-tone mask for optical and microelectronic applications,” *Microelectron. Eng*., vol. 23, no. 1-4, pp. 449–454, Jan. 1994.

[28] C. M. Waits, A. Modafe, and R. Ghodssi, “Investigation of gray-scale technology for large area 3-D silicon MEMS structures,” *J. of Micromech. Microeng.*, vol. 13, no. 2, pp. 170-177, March 2003.

[29] M. Woytasik, J.-P. Grandchamp, E. Dufour-Gergam, J.-P. Gilles, S. Megherbi, E. Martincic, H. Mathias, and P. Crozat, “Two- and three-dimensional microcoil fabrication process for three-axis magnetic sensors on flexible susbtrates,” *Sens. Actuators A, Phys*., vol. 132, no. 1, pp. 2–7, Nov. 2006.

[30] B. Morgan, C.M. Waits, and R. Ghodssi, "Compensated Aspect Ratio Dependent Etching (CARDE) using Gray-scale Technology," *Microelectronic Engineering*, Vol. 77, Issue 1, pp. 85-94, January 2005.

[31] B. Morgan, X. Hua, T. Iguchi, T. Tomioka, G. Oehrlein, and R. Ghodssi, "Substrate Interconnect Technologies for 3-D MEMS Packaging," *Microelectronic Engineering*, Vol. 81, pp. 106-116, July 2005.

[32] B. Morgan, J. McGee, and R. Ghodssi, "Automated 2-Axis Optical Fiber Alignment using Gray-scale Technology," *Journal of Microelectromechanical Systems (JMEMS)*, Vol. 16, pp. 102-110, 2007.

[33] B. Morgan, and R. Ghodssi, "Vertically-shaped Tunable MEMS Resonators," *Journal of Microelectromechanical Systems (JMEMS)*, Vol. 17, pp. 85-92, 2008.

[34] Y.-T. Lu, C.-S. Chu, H.-Y. Lin, "Characterization of the gray-scale photolithography with high-resolution gray steps for the precise fabrication of diffractive optics," *Opt. Eng*., vo. 43, no. 11, pp. 2666–2670, Nov. 2004.

[35] V. Kudryashov, X.-C. Yuan, W.-C. Cheong, K. Radhakrishnan, "Grey scale structures formation in SU-8 with e-beam and UV," *Microelectron. Eng*., vol. 67–68, pp. 306–311, June 2003.

[36] B. C. Morgan, "Electrostatic MEMS Actuators using Gray-Scale Technology," Ph.D. Dissertation, University of Maryland (2006).

[37] Gal, US patent 5,310,623 1994.

[38] H.-H. Kim, J.-Y. Yoo, S.-W. Park, Y.-K. Kwon, I. An, and H.-K. Oh, "A practical method for extracting the photoresist exposure parameters by using a dose-to-clear swing curve," *J. Korean Phys. Soc*., vol. 42, pp. S280-S284, Feb. 2003.

[39] M. LeCompte, X. Gao, and D.W. Prather, "Photoresist Characterization and Linearization Procedure for the Gray-Scale Fabrication of Diffractive Optical Elements," *Applied Optics*, vol. 40, no. 32, pp. 5921-5927, 2001.

[40] C. M. Waits, "Investigation of Gray-Scale Technology for Large Area 3D Silicon Structures," M.S. Thesis, University of Maryland (2003).

[41] B. C. Morgan, "Development of a Deep Silicon Phase Fresnel Lens Using Gray-Scale Lithography and Deep Reactive Ion Etching," M.S. Thesis, University of Maryland (2004).

[42] L. Mosher, B. Morgan, C. M. Waits and R. Ghodssi, "Advanced Techniques in 3D Photolithography for MEMS," *25th Army Science Conference,* Orlando, FL, USA, November 27-30, 2006.

[43] J.R. Sheats and B.W. Smith, "Microlithography: Science and Technology," *Marcel Dekker, Inc.*, New York, 1998.

[44] L. A. Mosher, B. C. Morgan, and R. Ghodssi, "Double-Exposure Gray-Scale Technology for Improved Vertical Resolution of 3D Photoresist Structures," *AVS 54th Intl. Symp.*, Seattle, WA, October 14 - 19, 2007.

[45] M. A. Fischler and R. C. Bolles, “Random sample consensus—A paradigm for model-fitting with applications to image-analysis and automated cartography,” *Commun. ACM*, vol. 24, no. 6, pp. 381–395, Jun. 1981.

[46] L. A. Mosher, C. M. Waits, B. Morgan, and R. Ghodssi, "A New Paradigm for High Resolution 3D Lithography," *Pro. IEEE MEMS 2008*, pp. 395-398, Tucson, AZ, USA, January 13-17, 2008.